Surface Oxidation of Millerite and its Galvanic Interaction with Chalcopyrite in Collectorless Flotation

By

Jing Han

A thesis submitted in partial fulfilment of the requirements for the degree of

Master of Science

In

Chemical Engineering

Department of Chemical and Materials Engineering

University of Alberta

ABSTRACT

Surface analysis of millerite and chalcopyrite were performed to enhance the understanding of fundamental millerite flotation behaviour in single mineral and mixed mineral conditions. By studying the mineral surfaces without collector addition, the ambiguity about the origin of the formed oxidative species can be reduced. This thesis investigates the flotation of millerite mineral and the surface species that form by using XPS, cyclic voltammetry and other qualitative methods. Millerite is closely associated with chalcopyrite in industry and is known to float with chalcopyrite in flotation circuits. Mixed flotation of the two minerals in collectorless conditions showed that depression of chalcopyrite occurred at pH 12. To understand the effect of millerite on chalcopyrite, rest potentials, XPS and ICP analysis of the two minerals were examined. It was found that chalcopyrite acted as the cathode, inducing further oxidation of the millerite. By studying the interactions between millerite and chalcopyrite, it was concluded that millerite had a depressive effect on chalcopyrite due to the galvanic interaction. Further tests with the addition of xanthate showed changes to the rest potential, resulting in a significant decrease in the difference between the two minerals. Therefore, galvanic interaction would not play a role if collectors were added. The results of this study provide fundamental understanding of millerite behavior in single and mixed mineral conditions.

ACKNOWLEDGEMENTS

I would like to give thanks to my supervisor, Dr. Qingxia (Chad) Liu for the opportunity to be a part of this exciting endeavour as well as the help and guidance that he provided throughout my research. I would like to express my gratitude towards Glencore and XPS for sponsoring the project. I would also like to thank the members of the nickel group for all the teamwork, ideas, and discussions that we have had that made this experience so much better. Special thanks to Dr. Rogerio Manica for editing and providing me with helpful suggestions.

Next, I would like to acknowledge the immense help the University of Alberta NanoFAB provided during my research. Without the help from Nancy Zhang, Shihong Xu and other staff members I would not have been able to get the results needed for my thesis. I would also like to thank Jim Skwarok for the help he has provided me in the lab.

Last but not least, I would like to express my utmost gratitude towards my family for all their support and encouragement that they have provided me.

Table of Contents

List of Figures

List of Tables

Chapter 1: Introduction

1.1 Introduction

Millerite (NiS) is a nickel sulfide mineral that can be found with chalcopyrite ($CuFeS_2$), bornite (Cu_5FeS_4) and pentlandite ($(FeNi)_9S_8$) in the Sudbury Basin, Ontario, Canada. The Sudbury Basin is one of the largest sources of nickel in the world. [1, 2] It also produces copper, cobalt, platinum and other precious metals, with wealth generated from the Sudbury Basin estimated to be about 160 billion US. [3]

The most common forms of nickel and copper sulphide is pentlandite and chalcopyrite, respectively. Nickel and copper are important minerals due to their versatility in properties and applications. Nickel is commonly used in the production of alloys such as stainless steel and are known to be resistant to heat and corrosion. [4, 5] Additionally, they are employed in the production of batteries and catalysts that make nickel extraction even more desirable. [4, 6] Copper is important because it is a good conductor of electricity and has high resistance to corrosion. Copper and its alloys are used in wires, piping and for agricultural purposes to name a few. [7, 8]

One of the companies that operate at the Sudbury Basin is Glencore. Glencore's Strathcona Mill in Sudbury produces a nickel-copper concentrate for smelting and a copper concentrate for smelting and refining. They are one of the largest producers and sellers of nickel and copper in the world. [9, 10]

Since millerite can be found with chalcopyrite, a method for adequately separating the nickel sulphide from the copper is desired. Flotation is used to separate the nickel and copper ores. Due to smelter regulations, the nickel percentage in the copper processing stream cannot exceed 0.6% [11] or a penalty is applied. A minimum copper grade of at least 20% is needed so that it can be processed in the smelter. [12] Strathcona Mill sets a target of achieving less than 0.5% nickel in their copper concentrate. The Strathcona Mill produced a nickel concentrate assaying around 16% nickel plus copper and a copper concentrate assaying 30% copper and 0.4% nickel in 2000. [13] A simplified flowsheet of the Strathcona Mill copper-nickel separation circuit can be seen in Figure 1.

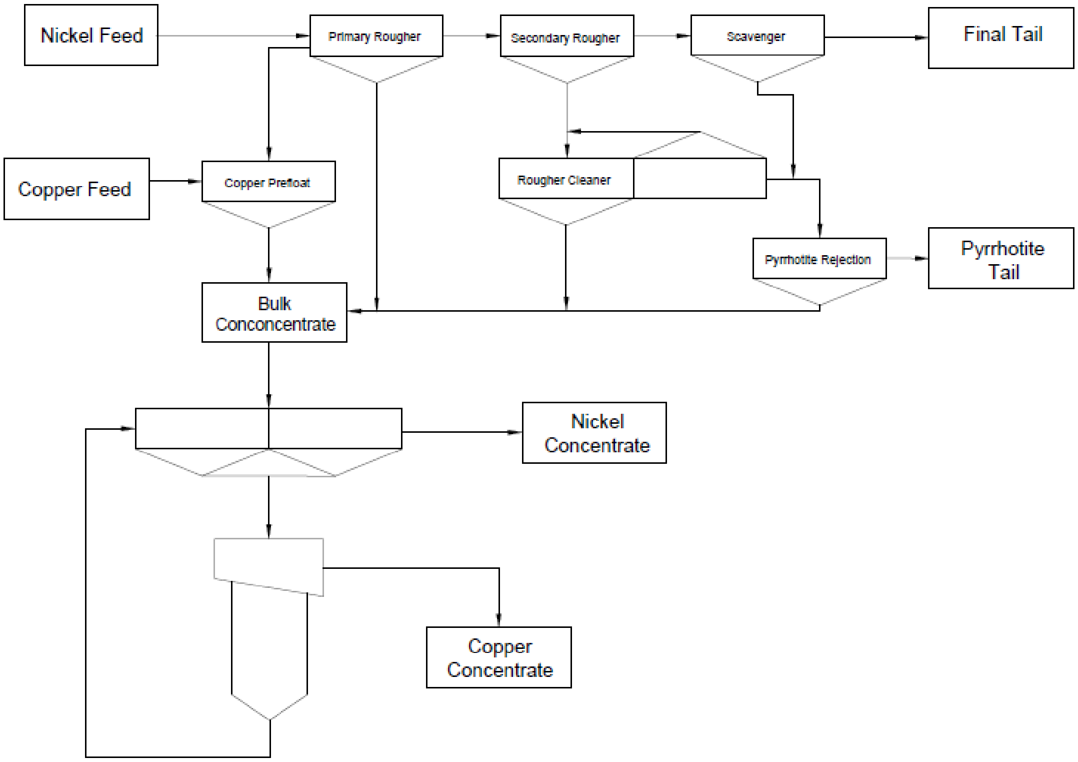

Figure 1. Copper-nickel separation circuit used in Strathcona Mill to produce nickel and copper concentrates from bulk concentrate.

The feed at the Strathcona Mill is split into nickel and copper feeds. The higher grade copper feed is first processed in a copper pre-float with the tails being combined with the nickel feed in the primary rougher. The tails of the primary rougher is then processed through a secondary rougher with the concentrate going into the rougher cleaner and the lower grade tails heading to the scavenger. The concentrate recovered from the scavenger is then brought to the pyrrhotite rejection resulting in the pyrrhotite tail and the concentrate is combined in the bulk. The bulk concentrate therefore consists of the concentrates from the pre-float, the primary rougher, the rougher cleaner and the pyrrhotite rejection. Lastly, nickel is depressed and collected as the nickel concentrate and the floated portion is collected in the copper concentrate. [14] This study will mainly focus on the portion following the bulk concentrate.

With continued excavation of the Sudbury Basin, millerite was found in copper-rich ores such as bornite and chalcopyrite. The millerite found in the Sudbury Basin is in massive form with noticeable cleavage points, possibly locked with chalcopyrite, bornite or pentlandite. Recently it was discovered that the nickel content had increased in the copper concentrate. The nickel species that predominately contributed to the increase was discovered to be millerite. [11] Misreporting of millerite to the copper concentrate was then identified, resulting in the desire to understand the flotation of millerite. As mining continues in the Sudbury Basin, copper resources will become depleted, leading to more impurities and other metals being mined. An increase in the presence of millerite could impact copper grades detrimentally and result in exceeding the cap of 0.5% that is targeted at Strathcona Mill. With limited prior knowledge regarding millerite, a fundamental understanding of its behavior becomes important. By studying the behaviours of millerite, methods of depression can be developed for future events where millerite is detected in the copper concentrate. Adequate separation of millerite from chalcopyrite is desired so that the value of nickel in the copper concentrate can be recovered, and the grade of the copper concentrate is not compromised.

1.2 Objectives

The main objective of this thesis is to understand millerite flotation, surface properties and species in a collectorless environment under single mineral conditions as well as in the presence of chalcopyrite. This will help provide the building blocks for depression of millerite in the copper concentrate through understanding how the surface changes in different conditions. By looking at the surface of the millerite in a collectorless condition, the surface interactions are more clearly defined. Galvanic interactions between millerite and chalcopyrite will be studied to see how oxidation influences their flotation behaviours. Lastly, how the addition of collectors impacts their flotation behaviours. From this study, surface species of millerite will be identified and this knowledge can be utilized to better develop methods of depression for millerite.

1.3 Overview of Thesis

For the selective separation of millerite from the copper concentrate to occur, it is essential to understand the flotation behaviour of millerite and how it interacts with other minerals. Chapter 1 will provide a brief introduction and an overview of the whole thesis. This is followed by literature review in Chapter 2, explaining the theory as well as the experiments and research performed on millerite or other sulphide minerals. The details of the experimental procedure are explained in Chapter 3. Chapter 4 presents an investigation of single mineral flotation in collectorless conditions and how the millerite surface transforms due to oxidation. The surface is studied using X-ray Photoelectron Spectroscopy (XPS) and contact angle measurements to understand the surface species affecting millerite flotation behaviour. The surface is also induced in oxidative and reducing conditions using cyclic voltammetry (CV) to study the changes of surface species that occur. Chapter 5 focuses on mixed mineral flotations between millerite and chalcopyrite, and explores the presence of galvanic interaction occurring between the two minerals. XPS, inductively coupled plasma mass spectrometry (ICP-MS) and other methods are used to study how the surface of both millerite and chalcopyrite changes. The fundamental knowledge will provide the necessary building blocks to establish a method to prevent the flotation of millerite in the copper concentrate. The thesis concludes in Chapter 6 and provides some insight for future experiments and studies.

Chapter 2: Literature Review

2.1 Introduction of Nickel Sulphides

Nickel is an important resource known for its high resistance to corrosion, versatility and its strength at high and lower temperatures. [4, 5] Due to its numerous applications, the extraction of nickel ores is desirable. The three main sources where nickel can be obtained are through the mining of laterite ore deposits and sulphide ore deposits, and through recycling of waste materials. [4, 5, 15, 16] Laterite ore deposits are further processed to produce ferronickel and alloys whereas sulphide ore deposits undergo flotation to produce nickel ore concentrates. [15] The nickel sulphide minerals that can be found in nature are: pentlandite ($(FeNi)_9S_8$), millerite (NiS), vaesite (NiS_2), polydymite (Ni_3S_4) and heazlewoodite (Ni_3S_2). [17] Other sulphide minerals that are commonly associated with these nickel sulphides are: chalcopyrite ($CuFeS_2$), bornite (Cu_5FeS_4), pyrite (FeS_2) and pyrrhotite ($Fe_{(1-x)}S$).

The ores found in the Sudbury Basin mainly consist of pyrrhotite, pentlandite and chalcopyrite usually disseminated in a norite host rock. The minerals found in nature show discrepancies from their ideal stoichiometric formula with substitutions such as cobalt found instead of iron and/or nickel. [18, 19]

The sulphides noted above that are of special importance are pentlandite and chalcopyrite for being the main sources of nickel and copper concentrates, respectively. Ideally, the separation of sulphide minerals would allocate the nickel minerals to the nickel concentrate and the copper minerals to the copper concentrate. However, this is rarely the case because the ideal condition for the flotation of one mineral can cause other minerals to be floated along with it due to overlapping similarities in properties. [15] The copper smelters in Canada have strict guidelines for the grade of the copper concentrate. If the nickel content is greater than 0.6%, then a penalty is dealt on the copper concentrate. [11] The value of the nickel is lost in the process as well. The need for selective separation of sulphide minerals is crucial for the industry. The key is to understand the surface changes and mineral interactions that occur during flotation.

2.2 Importance of Millerite

While millerite is not the most prominent of the nickel sulphides recovered, its importance has increased due to its unique properties. There are two main types of millerite: one that can be found in nature, β-NiS (Figure 2) and one that can only be found at high temperatures (above 400°C), α-NiS. [19, 20, 21] The nickel-sulphur species existing at different temperatures and sulfur contents can be seen in Figure 3 [22] and the main focus of this study will be on β-NiS.

Figure 2. Piece of Sudbury millerite from Levack Mine, obtained from Kaygeedee Minerals. The millerite is shown in the middle in brassy yellow with the darker gold being chalcopyrite.

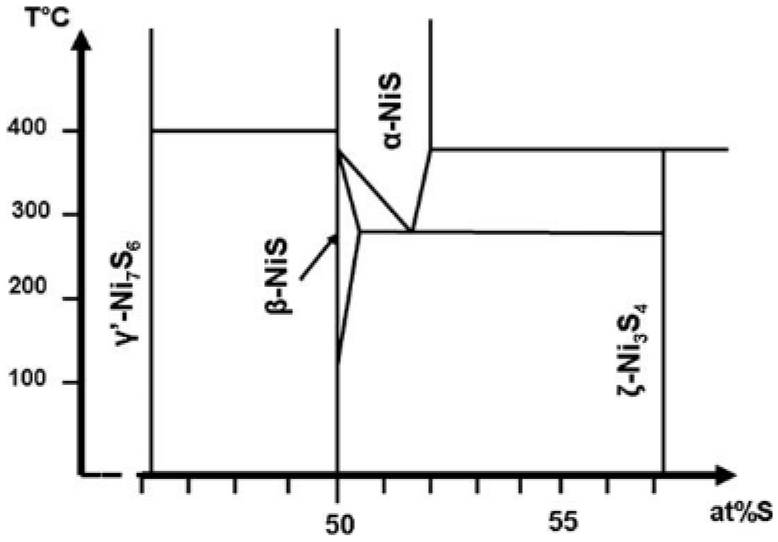

Figure 3. Nickel sulphide species existing at various sulfur atomic percentages as a function of temperature. α-NiS appears only at high temperatures while β-NiS can be found in nature. [22]

There are different uses for both types of millerite. α-NiS can be utilized as a catalyst for hydrogenation and hydro-sulphurization. [23, 24] The β-millerite contains a nickel content of 64%, greater than that of pentlandite which only has 34%. Both millerites are also known for their useful electrochemical properties, good electrical conductivity and low cost. α-millerite is a better conductor and is unlikely to form nickel hydroxides in alkaline solutions. The synthetic production of both millerite species is being investigated and applied. [25], [26] Another application for millerite is its use in rechargeable lithium batteries. The β-millerite found in nature can appear in two different crystal aggregates, often appearing in needle-like structures (Figure 4) or solid sheets with clear cleavage points. The millerite found in the Sudbury region consists of shiny layered sheets that can be easily cleaved.

Figure 4: Acicular needle-like form of millerite that occurs naturally. This piece was found in the Sterling Mine in New York, United States. [27] The millerite found in the Sudbury Basin are not of this shape.

2.3 Millerite Compared to Pentlandite

Recovery of millerite is important because it contains one of the highest nickel contents at 64%, whereas pentlandite only contains 34% nickel. [11]

Smith et al. (2011) compared millerite flotation with pentlandite under xanthate collector conditions at pH 9. [28] From Figure 5, it can be seen that pentlandite has a slightly higher recovery compared to millerite. With an increase in pH, Smith et al. noted that both millerite and pentlandite further decreased in recovery.

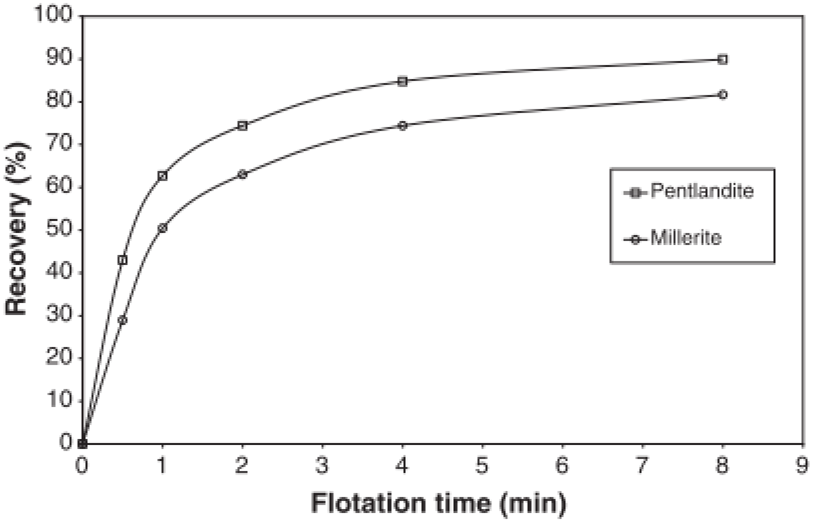

Figure 5. Flotation comparison of millerite and pentlandite at pH 9 with 120 g/t KEX

The current method used to adequately depress the pentlandite to the nickel stream using cyanide was found to be ineffective when applied to millerite. Smith's flotation tests showed that millerite only depressed when high concentrations of cyanide was used which is unpractical in an industrial setting. [28] The exact mechanism behind cyanide depression is unclear but it has been hypothesized that depression occurs through altering the actions of xanthate on the mineral surfaces. [29] The formation of hydrophilic iron cyanide surface compounds inhibits the adsorption of xanthate leading to depression. Senior et al. (2009) [30] proposed the mechanism for cyanide depression of gersdorffite as being represented by Equation 2.1:

$$Ni(OH)_2 + 4CN^- = Ni(CN)_4^{2-} + 2OH^- \tag{2.1}$$

This mechanism would explain the high concentrations of cyanide required to depress millerite since no iron cyanide complexes would be formed, unlike that of pentlandite.

2.4 Sulphide Oxidation

2.4.1 General Sulphides

When sulphide surfaces are exposed to air, the surfaces undergo oxidation. Oxidation is the process where the surface of the mineral loses electrons while the other component gains electrons to become reduced. For sulfide minerals, the extent of oxidation on the surface plays a great role on its flotation behaviour. It has a direct impact on the bubble-particle attachment during flotation, affecting flotation recovery. [31] The mineral surface will change as a result of oxidation, resulting in the formation of a passivation layer. [32] The formation of a passivation layer could cause the inhibition of bubble attachment resulting in the decrease of flotation recovery. The oxidation on sulphide minerals begins with the dissolution of metal ions into the solution to produce either metal deficient sulfides or metal hydroxides. [15, 31] It was determined that elemental sulfur on the surface imparts a hydrophobic effect that helps to promote the collectorless flotation of metal sulfides. [34] One of the factors that has a direct effect on oxidation is the pH of the solution. pH is a measurement of the concentration of hydrogen ions in the solution. [35] The typical reactions for the oxidation of metal sulfides in acidic and alkaline conditions are given as Equations 2.2 and 2.3, respectively [36].

$$MS \rightarrow M^{n+} + S^0 + ne^- \tag{2.2}$$

$$MS + nH_2O \rightarrow M(OH)_n + S^0 + nH^+ + ne^- \tag{2.3}$$

These two reactions only occur when slight oxidation of the surface has occurred. [34] With increased surface oxidation, the sulfur can further undergo transformation into sulphates causing the surface of the mineral to become hydrophilic. The corresponding reactions are represented by Equation 2.4 and/or Equation 2.5.

$$S^0 + 4H_2O \rightarrow SO_4^{2-} + 8H^+ + 6e^-$$

(2.4)

$$2S^0 + 3H_2O \rightarrow S_2O_3^{2-} + 6H^+ + 4e^- \qquad (2.5)$$

Oxidation can greatly affect the behaviour of sulphide minerals and must be taken into account when designing flotation experiments. [37] There is a fine balance when it comes to sulphide oxidation. A 5% oxygen gas flotation showed a higher recovery and selectivity when compared to using air. [15] This shows that flotation recovery decreases when the surface of sulphide minerals is heavily oxidized.

The presence of sulphate formation during sulphide flotation is uncommon due to excessive oxidation required over a long period of time to form stable sulphates. This time is much longer than the expected flotation time. [38] The presence of sulphates can therefore be explained by the existing oxidation that has already occurred on the mineral surface if no oxidants were added.

2.4.2 Millerite

With slight oxidation of the millerite surface, surface sulfur is exposed due to the release of nickel ions into solution (Equation 2.6). The reaction in acidic conditions can be described by the following equations: [30, 37, 38, 39]

$$NiS \rightarrow Ni^{2+} + S + 2e^-$$

(2.6)

$$NiS + 4H_2O \rightarrow Ni^{2+} + SO_4^{2-} + 8H^+ + 8e^-$$

(2.7)

At high pH, the nickel ions react to form nickel hydroxides which are deposited back on the surface of the mineral as precipitates. The nickel speciation diagram can be seen in Figure 6. [42]

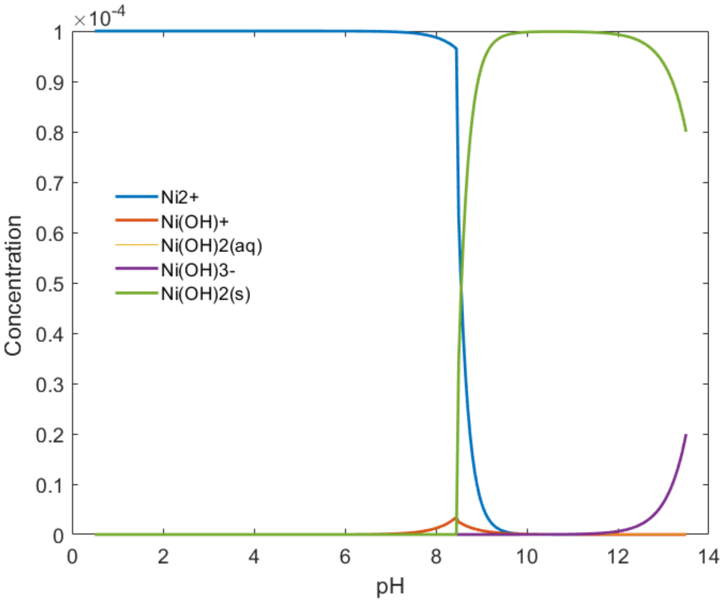

Figure 6. Speciation diagram for nickel at different concentrations as a function of pH. [42]

The proposed oxidation process of millerite at different degrees of oxidation can be seen in Figure 7. Due to the presence of sulfur, the surface of the millerite is slightly hydrophobic in this case. As oxidation increases, the surface sulfur reacts with oxygen to form sulfates causing the surface to become more hydrophilic.

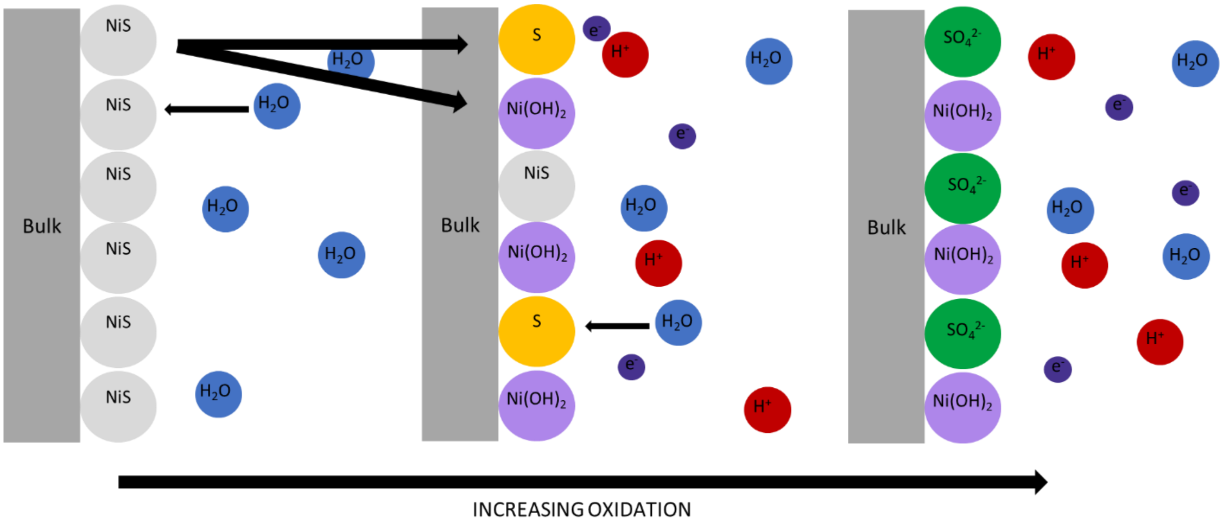

Figure 7. Millerite surface changes with increasing degree of oxidation in alkaline conditions. This image shows the oxidation of NiS to surface sulfur and in the presence of further oxidation to soluble sulphate.

2.4.3 Chalcopyrite

Oxidation of chalcopyrite has been thoroughly studied by numerous researchers. [38, 42] The oxidation of chalcopyrite follows the same mechanism as the oxidation of other sulphide minerals. It does not exhibit fast oxidation rates and it begins with the release of ferric ions which forms soluble ferric hydroxides or oxides in alkaline conditions following Equation 2.8. [31, 41] The copper in chalcopyrite is less likely to be released thus forming CuS.

$$CuFeS_2 + 3H_2O \rightarrow Fe(OH)_3 + CuS + S + 3H^+ + 3e^-$$

(2.8)

With further oxidation of CuS following Equation 2.9:

$$CuS + 2H_2O \rightarrow Cu(OH)_2 + S + 2H^+ + 2\,e^- \qquad (2.9)$$

The formation of CuS and soluble $Fe(OH)_3$ as a result of mild chalcopyrite oxidation causes the surface to become more hydrophobic, increasing its affinity for bubble attachment. In the presence of higher oxidation conditions, the presence of metal hydroxides on the surface of copper sulfides will inhibit their flotation even with the addition of collectors. [33]

2.5 X-ray Photoelectron Spectroscopy

X-ray photoelectron spectroscopy (XPS) is widely used in the identification and quantitative analysis of surface layers with measurements averaging 5 nm in depth. [45] X-rays are beamed on the sample surface, exciting photoelectrons. This causes the photoelectrons to leave the surface and are measured, relaying information about its binding energy. Based on the binding energies observed, it is possible to determine which elements exist as well as their chemical state.

Legrand et al. (1998) [46] used x-ray photoelectron spectroscopy (XPS) to analyze millerite under different conditions to determine surface species. They sought to consolidate the binding energies of millerite due to ambiguous results in the literature and similarities in binding energy of sulfur species. They tested the fresh surface of millerite, air exposed millerite for 24 hours and for one year, as well as submerging it into distilled water. Through their experiments, they noticed that there was hydroxide formation even in the event of cleaving the millerite under high vacuum conditions, exposing fresh surfaces. This means that millerite is very sensitive to air. An increase in the amount of hydroxide was seen when the millerite was submerged in water. Due to similar binding energies of sulfide and polysulfide species, they could not be distinctively identified using XPS. However, Legrand believed that there was a clear indication of sulfates existing on the surface of the mineral.

2.6 Rest Potential and Pulp Potential

The flotation of sulphide minerals is greatly affected by both the rest potential and the pulp potential. Oxidation/reduction potential (Eh) is used to signify the potential of the minerals and is typically measured using a three-electrode system. The electrochemical system includes a reference electrode so that readings can be calculated and represented using the standard hydrogen electrode scale so that experiments between different researchers can be compared. Platinum electrodes were found to be more sensitive to the oxygen content in pulp, whereas gold electrodes were not significantly affected. [44, 45] Therefore, gold electrodes should be used in situations where oxygen interference needs to be reduced. Along with the material selected for the electrode, the shape of the electrode should also be taken into account. Shapes that result in increased contact with the particles will produce measurements more representative of the particles than the solution.

Rest potentials are measured using a mineral electrode, which is representative of the mineral's redox reaction with water. By knowing the rest potentials of individual minerals, the possibility of galvanic interactions can be theorized. [49] If there are multiple electrodes present, the measurement taken is representative of the mixed potential (pulp potential), which is the equilibrium of two or more redox reactions occurring. By altering the pulp potential, the oxidative species on the surface could possibly be controlled. [48] The Nernst equation [50] represents the potential required for a redox reaction (Equation 2.10) to occur based on the concentrations of the ions being reduced and oxidized as shown in Equation 2.11.

$$aOx + ne^- \leftrightarrow bRed \tag{2.10}$$

$$E_{Ox/Red} = E^o_{Ox/Red} - \frac{RT}{nF} ln \left\{ \frac{A^b_{Red}}{A^a_{Ox}} \right\} \tag{2.11}$$

where $E_{Ox/Red}$ is the reduction potential of the reaction, $E^o_{Ox/Red}$ is the standard reduction potential, *R* is the gas constant, *T* is temperature in K, *n* is the stoichiometric number of electrons in the reaction, F is the Faraday constant, *a* is the stoichiometric coefficient of the oxidized species, *b* is the stoichiometric coefficient of the reduced species, A^b_{Red} is the activity of the reduced species and A^a_{Ox} is the activity of the oxidized species. [51]

By calculating and plotting the Nernst equation, it is possible to predict what species are present and predict which species cannot exist. Figure 8 shows the Pourbaix diagram that Stamboliadis (1976) created for millerite and its associated species. [52]

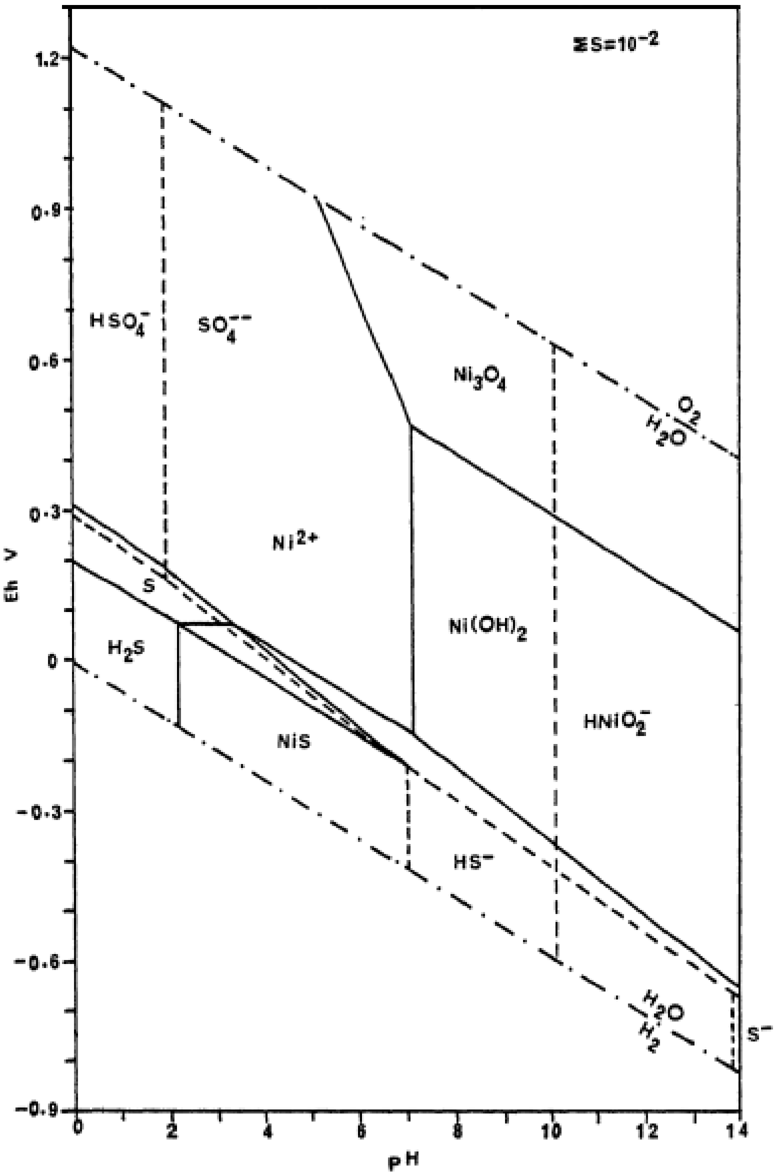

Figure 8. Pourbaix diagram for millerite species with pH as a function of Eh. [52] The diagram was calculated using concentrations of 10^{-2} M for both Ni and S. This diagram helps to predict the possible surface transformations that occur to millerite during flotation while controlling the pH and monitoring the Eh.

The pulp potential is mainly modified through the use of chemical oxidants/reductants or by applying potential through an external source. [48]

2.7 Galvanic Interaction

Galvanic interaction is an important part of flotation caused by a difference in rest potential between two dissimilar metals. [37, 38] The mineral with the higher rest potential is known as the cathode and will undergo reduction in galvanic interaction. The mineral with the lower rest potential is the anode and will undergo oxidation. [36, 50] The equation of the reaction at the cathode can be represented by Equation 2.12. [54]

$$\frac{1}{2}O_2 + H_2O + 2e^- = 2OH^+ \qquad \text{Equation 2.12}$$

Due to sulphide minerals being semi-conductive, the reduction/addition of oxidative products on the surface will drastically affect how the mineral behaves in flotation. [39] The main effects of galvanic interaction between two minerals are at high pH: surface passivation, metal ion migration causing the formation of hydroxides, ion activation and differences in area spurring oxidation formation. [38, 51] Galvanic interaction not only occurs during flotation. The effect of the grinding media onto the mineral during the grinding process will also impart galvanic effects. [40]

Xia et al. [56] studied the effect of galvanic interaction between pyrite and sphalerite by measuring the migration of added copper ions and its interaction with xanthate. They used two different setups to test the effects of galvanic interaction – one where the pyrite and sphalerite are mixed in a reactor and another setup where they share the same circulating fluid but are kept apart. They hypothesized that the copper ions would activate the pyrite as well as the sphalerite but when experiments were conducted, there was noticeable depression of the pyrite. By using UV spectroscopy, they were able to tell that the copper preferentially adsorbed on the sphalerite when it was in contact with pyrite. This did not occur when sphalerite was not mixed with pyrite. This result showed that, due to galvanic interaction, copper was more likely to adsorb onto sphalerite and as a result created a more stable complex with the xanthate allowing sphalerite to be floated. The preferential adsorption caused pyrite to adsorb less xanthate as a result, leading to its depression.

2.8 Flotation Behaviour of Millerite

The flotation behaviour of millerite has not been thoroughly studied, with only a few experiments about it. Smith et al. (2011) [28] studied the flotation of millerite and how it compared with pentlandite since both minerals are nickel sulphides. Millerite depression is of special interest so that separation from chalcopyrite can occur. In his experiment, Smith showed that millerite did not respond to the addition of cyanide, which is commonly used to depress pentlandite, and only showed effects when high concentrations of cyanide were added. It was concluded that cyanide would not be a great option as a depressant for millerite. Smith also conducted experiments that showed millerite floated with 80% recovery when xanthate collector was added. His experiments were only limited to single mineral flotation.

Xu et al. [11], working for Vale, reported that there was an increase of nickel in the copper concentrate that resulted in a copper concentrate that was close to the limit. They discovered that the copper rich ores in the Sudbury Basin were more likely to carry millerite along with the chalcopyrite. Although there was more pentlandite mixed in with the chalcopyrite, due to the higher nickel content of millerite, it significantly contributed to the nickel grade in the copper concentrate. In their study, they investigated ways to depress millerite by using cyanide, starch and dextrin. They showed that starch and dextrin did have a depressing effect on the nickel, but dextrin was also causing a depressing effect on the chalcopyrite. The exact depression mechanics were not explored, but Xu et al. suggested that the reason for the depression could be either sensitivity as a result of the dosage or from the uncontrollable degree of oxidation.

2.9 Cyclic Voltammetry

Cyclic voltammetry has been used quite commonly to determine the surface oxidation reactions occurring on minerals. The basic guide for cyclic voltammetry was summarized by Elgrishi et al. explaining how to interpret the peaks in the oxidizing and reducing regions. [57]

Power [32], [58] investigated the effect of synthetic NiS cyclic voltammetry under acidic conditions using a synthetic rotating nickel sulfide electrode. Previous investigations of nickel sulfide oxidation suggested that passivation layer was mainly caused by the formation of nickel hydroxides or oxides. Through his work, Power discovered that the main reason for the anodic passivation of nickel sulfide was the presence of nickel deficient sulfides as well as elemental sulfur in acidic conditions.

Combining cyclic voltammetry with Pourbaix diagrams is a helpful technique to understand the reductive and oxidative species forming on the surface of minerals.

2.10 EDTA Extraction

Ethylenediaminetetraacetic acid (EDTA) is used to extract mineral oxides and hydroxides without causing the leaching of the bulk mineral in a deoxygenized alkaline environment. Research done by Rumball and Richmond (1996) [59] and Clarke *et al.* (1995) [60] showed that EDTA extraction is capable of removing freshly oxidized metal species and that dissolution would take much longer for aged oxidized metal species. Rumball hypothesized that EDTA extraction for 1 hour would only remove approximately 80% of oxidized metals. EDTA extraction has also been used by researchers to measure the change in oxidation under different experimental conditions.

Chapter 3: Experimental

3.1 Millerite and Chalcopyrite Samples

The millerite obtained for experiments was purchased from Kaygeedee Minerals, originating from the Sudbury Region. The chalcopyrite was purchased from Wards Scientific. The large chunks of minerals were first broken down using a jaw crusher. The minerals were then handpicked and grinded by using a mortar and pestle. They were separated by using RO-TAP and sieved to obtain 75 µm to 38 µm fraction for flotation use. They were then sonicated and washed with distilled water until the fines were washed out. [60] The remaining smaller than 38 µm fraction was used for inductively coupled plasma mass spectrometry experiments (ICP-MS). The samples were then dried using a FreeZone freeze dryer and stored in a freezer in aluminum bags filled with nitrogen gas to avoid additional oxidation.

Rigaku XRD Ultima IV was used for X-ray powder diffraction (XRD) to identify the species existing in the millerite ore. From Figure 9, the millerite sample obtained mainly consists of millerite and a slight trace amount of chalcopyrite. The purities of the feed samples were tested by using Orbis PC Micro-EDXRF Elemental Analyzer for X-ray fluorescence (XRF) analysis. Prior to the analysis, the samples were further grinded with a mortar and pestle to ensure the powders were homogeneous. Three readings were taken at different points on the sample and averaged for the results. Silica was detected as an impurity, but the results were omitted in the calculations. The XRF results of the powdered feed samples for millerite and chalcopyrite can be seen in Table 1. The purity calculated based on the molecular weights was 89% for the powdered millerite and 98% for the chalcopyrite sample. This means that the chalcopyrite sample has a high purity, so no further identification analysis was conducted.

Table 1. XRF analysis for the purity of powdered Sudbury millerite feed and chalcopyrite samples. The scan was conducted three times and then averaged to obtain the weight percent.

	Weight %				**Purity %**	
Mineral	**S**	**Fe**	**Ni**	**Cu**	**Millerite**	**Chalcopyrite**
Millerite	36.6	3.7	57.5	2	89	6.2
Chalcopyrite	36.3	28.7	0.05	34.2	N/A	98.7

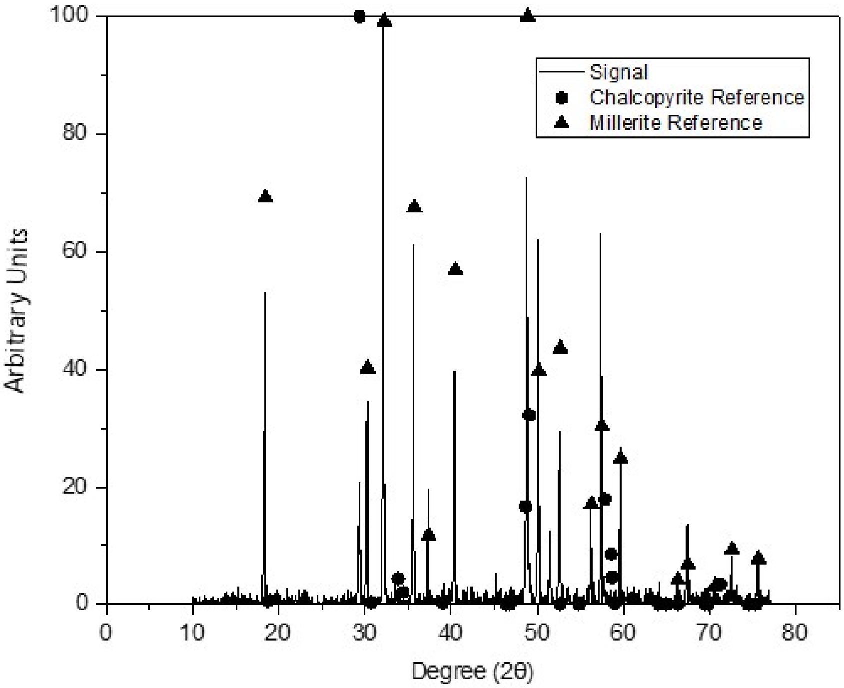

Figure 9. Rigaku XRD pattern of the Sudbury millerite powder used as feed for experiments. The circles represent the reference for chalcopyrite and the triangles represent millerite. The sample displayed the presence of both minerals.

Mineral electrodes were made from solid pieces of millerite and chalcopyrite connected by wire using silver conductive glue and then set in epoxy and polished until the surface was exposed. Two sizes of circular electrodes were made, one with a diameter of 5 mm used for rotating/stationary cyclic voltammetry and mixed mineral experiments and another with a diameter of 3 cm for analyzing contact angle and EDTA extractions due to the larger surface area. The electrodes were analyzed with a scanning electron microscopy with energy dispersive X-ray spectroscopy (SEM/EDX) to determine the elemental content (Table 2, Table 3, and Table 4) of the electrode surface and images can be seen in Figure 10, Figure 11 and Figure 12. Slight impurities of bismuth were detected on the chalcopyrite and silica, and iron was detected on the millerite electrode.

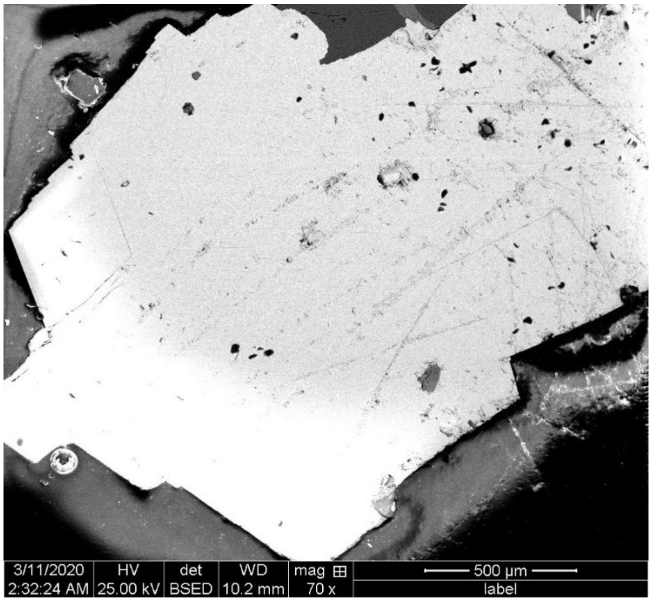

Figure 10. SEM image of 5 mm millerite electrode used in electrochemical experiments

Table 2. SEM-EDX analysis of the elemental content in the 5 mm millerite electrode

Element	wt%	at%
Ni	53.8	38.9
S	46.2	61.1

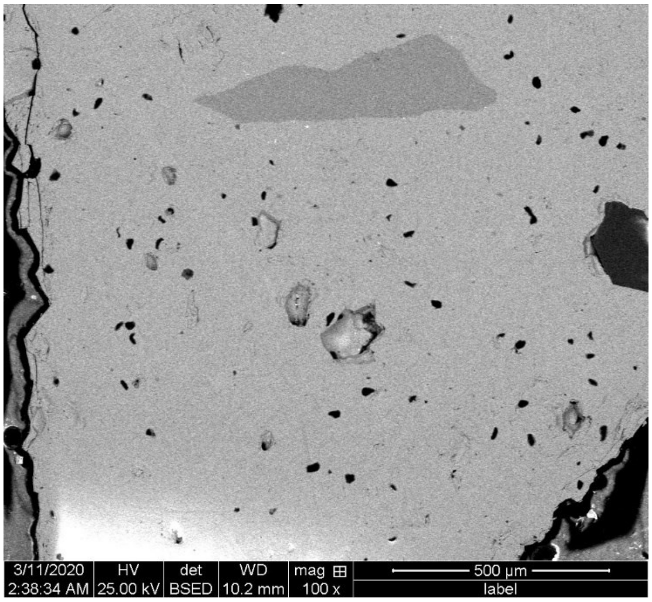

Figure 11. SEM image of 5 mm chalcopyrite electrode used in electrochemical experiments

Table 3. SEM-EDX analysis of the elemental content in the 5 mm chalcopyrite electrode

Element	wt%	at%
Cu	27.5	19.1
S	39.9	55.1
Fe	32.6	25.8

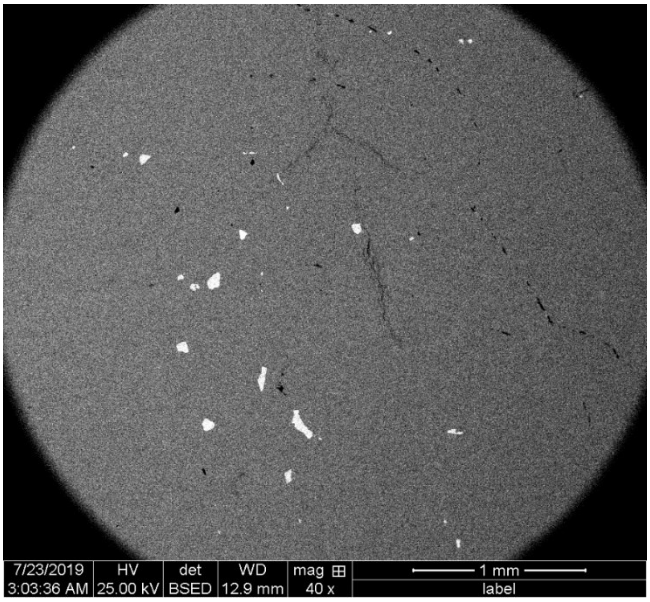

Figure 12. SEM image of 3 cm chalcopyrite electrode used in electrochemical experiments

Table 4. SEM-EDX analysis of the elemental content in the 3 cm chalcopyrite electrode

Element	wt%	at%
Cu	37.1	27.2
S	32.6	47.4
Fe	30.4	25.4

3.2 Micro-flotation Setup

Micro-flotation experiments were performed due to limitations in the availability of millerite. Each micro-flotation experiment used around 1.4 g for single mineral flotation, 0.7 g of each mineral for mixed flotations. The samples were sonicated for 5 minutes prior to flotation in separated containers before being combined and then conditioned for another 5 minutes. The mixed flotation concentrates and tails were measured using XRF analysis to determine the percentages of millerite and chalcopyrite recovered. No collector was added in these experiments, opting for a fundamental understanding of the behavior of millerite, unless otherwise stated.

A portion of the -38 μm fraction obtained from grinding was further pulverized using a McCrone micronizing mill for 10 minutes to obtain less than 10 μm fraction to be used in galvanic conditioning experiments.

The micro-flotation setup can be seen in Figure 13 with the ability to measure the pulp potential as the experiments are conducted using a 3-electrode setup. The flotation cell consists of four different parts. The sample is placed in the bottom portion and is also where the tails can be collected after flotation has occurred. The two sides are connected to the bottom part using ground glass joints, allowing the movement of solution but not particles. The reference electrode and the counter electrode are placed in the side portion. Lastly, the top portion is where the concentrate is collected, and the platinum mesh is secured. This setup was used for both the single mineral flotation as well as the mixed mineral flotations.

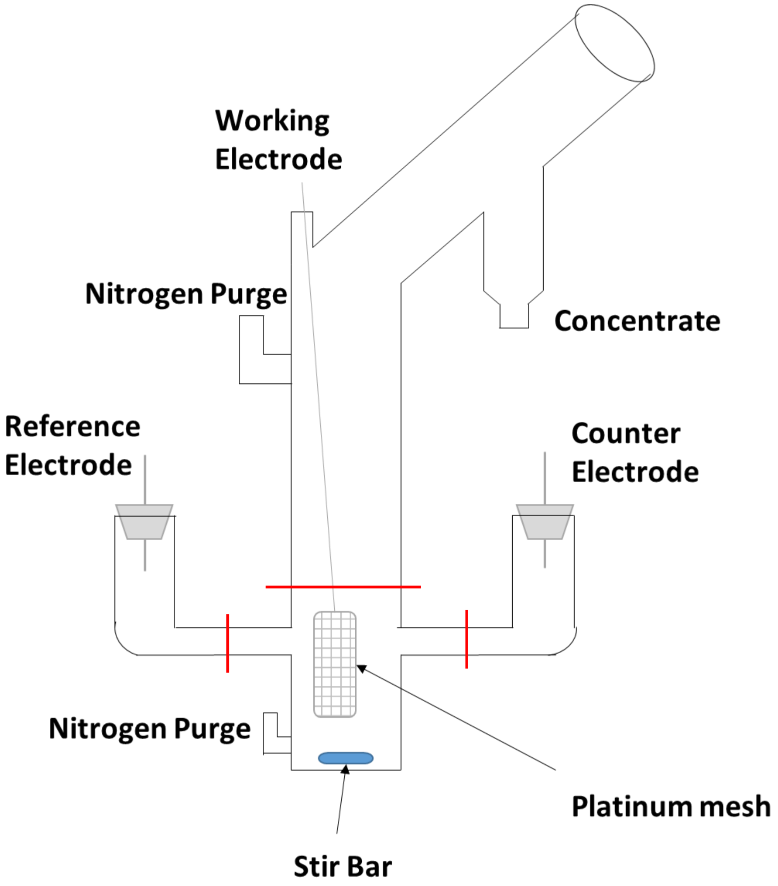

Figure 13. Schematic of the electrochemical micro-flotation cell used for flotation experiments. The red lines indicate joints where the flotation cell is assembled.

The reference electrode used for the experiments is a calomel electrode and results were corrected to standard hydrogen electrode (SHE) by adding 245 mV so that results can be compared to the literature. [50] The counter electrode and the working electrode are both made from platinum mesh. They are connected to a CH Instruments Electrochemical Analyzer potentiostat that records the potential using CHI 600e software throughout the experiment.

The flotation system is clamped and mounted above a stirring plate. The flotation cell holds 140 mL of liquid. The stir bar is placed at the bottom and held at 1100 RPM during conditioning stages and decreased to 700 RPM during flotation. There are two nitrogen purge inlets for the setup. The upper inlet is used to keep a purged environment during the conditioning process and the bottom inlet is used to induce flotation. The nitrogen flowrate is controlled at 20 SCCM by a Cole-Parmer flow meter during flotation. The flotation setup is washed thoroughly between experiments.

The ground glass joint connection prevents the mineral from floating into the electrode areas while monitoring the pulp potential. The conditioning time was kept at 5 minutes with another 5 minutes for the flotation process. NaOH and HCl were used to modify the pH to the desired value. The solution pH was monitored throughout the experiment and adjusted accordingly.

3.3 Cyclic Voltammetry and Rest Potential Setup

The setup of the cyclic voltammetry and rest potential measurements can be seen in Figure 14. The reference electrode is a calomel electrode and the counter electrode, a platinum mesh. The experiments were conducted by rotating the mineral electrode at 2000 RPM or in stationary conditions using a Pine Rotating Disk Electrode. The solution was purged with nitrogen for 15 minutes prior to each experiment. Addition of sodium tetraborate was used in pH 9 solutions to act as a buffer. No additional buffers were added for pH 12 due to its stability from the high concentration of NaOH added. The surface of the electrodes was polished using 600 grit, 800 grit, 1200 grit silicon carbide sandpaper and then micro-polishing cloth followed by 5-minute sonication to ensure a smooth surface was achieved. The cyclic voltammetry experiments were scanned three times, either in the reducing or oxidizing direction. The rest potential measurements were kept constant for 1 hour ensuring that equilibrium could be reached.

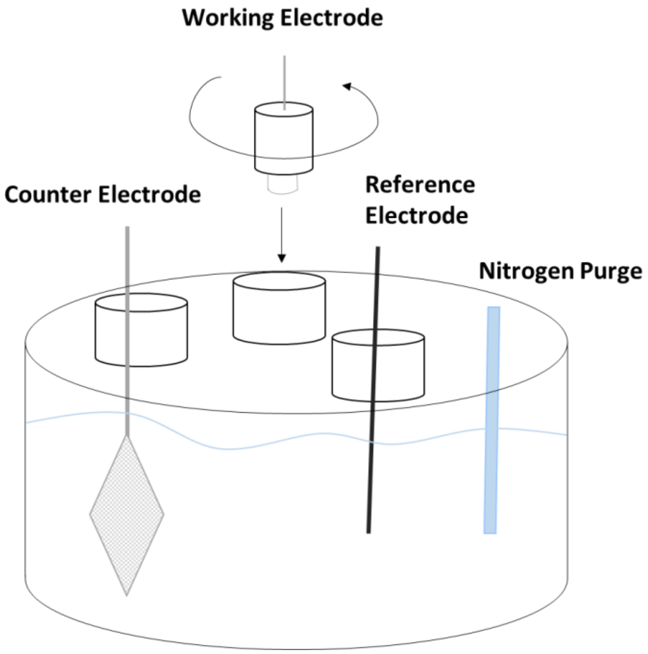

Figure 14. Schematic of the cyclic voltammetry and rest potential setup using Pine Rotating Disk Electrode. The reference electrode is a calomel electrode and the counter electrode is a platinum mesh.

The calculation for reactions that occurred during the CV scan were determined using the Nernst Equation (3.1) and Gibbs free energy (3.2):

$$E_{cell} = E^{\circ}_{cell} - \frac{RT}{nF}\ln Q \tag{3.1}$$

$$\Delta G^{\circ} = -nFE^{\circ}_{cell} \tag{3.2}$$

The Gibbs free energy was calculated for oxidative reactions using the chemical potentials for each component from Gamsjäger et al. (2005) [61] and by assuming solution concentrations to be 1 M.

3.4 XPS Sample Preparation

For the single mineral x-ray photoelectron spectroscopy (XPS), Kratos AXIS Ultra XPS was used to complete the scans. The sample for XPS analysis was prepared from the feed sample conditioned and stirred at the specified pH for 1 hour. Prior to the conditioning, the sample was sonicated for 5 minutes. During the experiment, the pH was continuously monitored and adjusted using NaOH. The solution was purged with nitrogen prior to adding the minerals and through the duration of the process. After 1 hour, the solution was decanted, and the remaining minerals were rinsed with distilled water. The solution was then stored inside the fridge until frozen and then freeze-dried to obtain the sample for XPS.

The mixed mineral samples used PHI VersaProbe III Scanning XPS Microprobe for analyzing the surfaces. This XPS allows the user to view an image of the surface and determine where they would like to scan whereas the Kratos AXIS Ultra cannot. The mixed samples used an electrode conditioned with -38 µm mineral powders for 1 hour in purged pH adjusted solution.

3.5 EDTA Extraction and ICP Preparation

Single mineral and mixed mineral dissolution samples were prepared by stirring powdered minerals for 1 hour under purged conditions, and then using a 0.25 µm filter syringe to extract the solution.

The preparation of EDTA extraction was based on Rumball (1996) and used the same concentrations. Nitrogen was purged throughout the preparation of the EDTA solution. NaOH pellets were added to the EDTA solution until the solution cleared, further addition of NaOH was used until the pH was adjusted to 9. In the extraction of surface metal hydroxides from the metal electrode, the electrode was first conditioned in pH 12 water for 1 hour before the electrode was rinsed with pH adjusted solution to remove any residue particles before being transferred into EDTA solution.

Chapter 4: Surface Oxidation

4.1 Single Mineral Micro-flotation Results for Millerite

To have a clear understanding of the behaviour of millerite, single mineral micro-flotation experiments were conducted without the use of flotation modifiers. The results for the single mineral flotation of millerite can be seen in Figure 15. From the graph, without the addition of collector, millerite is only slightly floatable in purged conditions. The recovery at pH 4, 6 and 9 was found to be around 27%. The flotation recoveries in acidic and slightly alkaline solutions did not change by much and repeated experiments produced small error bars. At pH 12, the recovery dipped down to 15%, which is almost half of what was recovered at pH 9. The pulp potential was highest at pH 4 with 0.309 V and lowest at pH 12 at 0.06 V.

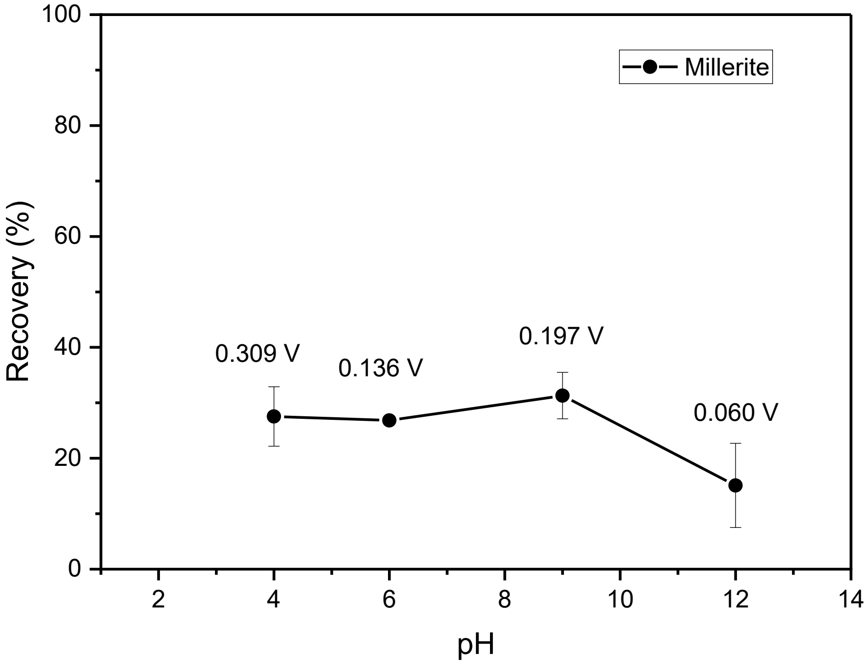

Figure 15. Collectorless single mineral flotation of millerite at pH 4, 6, 9 and 12 with pulp potential measured in SHE.

It is hard to conclude from just looking at the flotation recoveries and pulp potentials what is causing the millerite flotation behaviour to decrease at pH 12. Additional experiments were conducted to study the surface species of millerite at pH 9 and 12 to replicate industrial conditions.

4.2 XPS Results for Millerite

X-ray photoelectron spectroscopy (XPS) was used to study the surface conditions for the feed sample, as well as millerite samples conditioned at pH 9 and pH 12. XPS was used to analyze the binding energy released as photoelectrons are ejected from the surface by x-rays. The pH 9 and 12 samples were selected because they are reflective of plant conditions. The results for the overall scans of the millerite surface can be seen in Figure 16 and a breakdown of the elemental area coverage is given in Figure 17. The narrow scans for nickel, oxygen, carbon and sulfur content were also conducted for each condition. Deconvolution of the data mainly focused on the nickel and sulfides. Due to the complexities of the oxygen species, they were omitted. The data was calibrated using the obtained carbon peaks and then fitted using the carbon to carbon binding energy of 284.8 eV (Thermo Fisher Scientific). From Figure 14 and Figure 15, it can be seen that the surface oxygen content increased as the pH was increased. The sulfur signal for all three samples were weak but there was a slight decrease as the pH was increased.

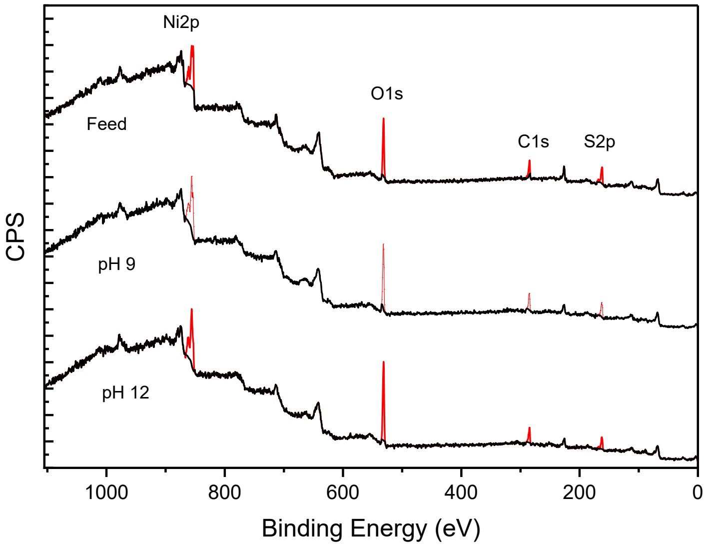

Figure 16. Survey scans for millerite feed and millerite samples conditioned at pH 9 and pH 12. The black lines are representative of the background and the red lines are the peaks for Ni 2p, O 1s, C 1s and S 2p from left to right.

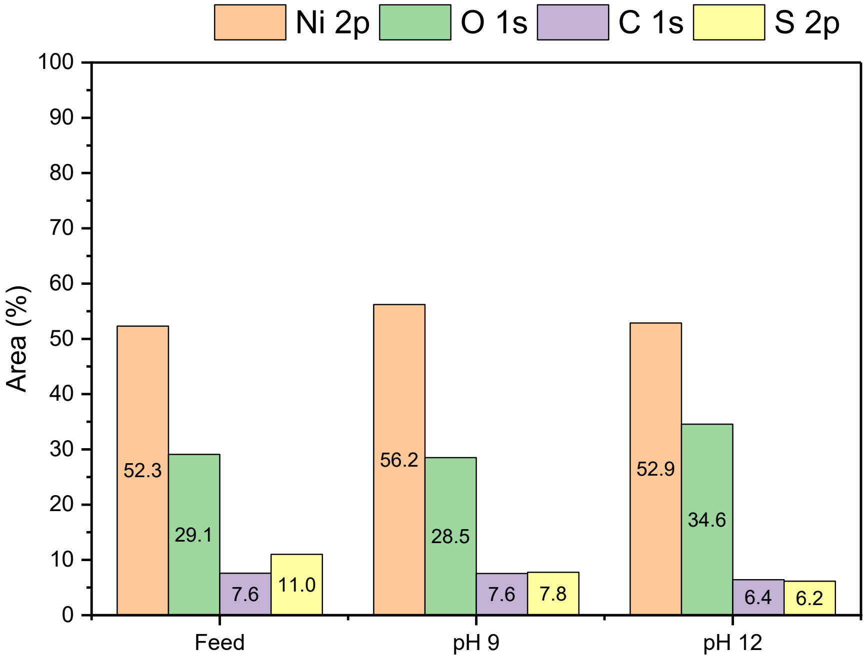

Figure 17. Breakdown of elemental surface coverage from XPS survey scans of millerite feed and millerite conditioned at pH 9 and pH 12. The colors represent: orange for nickel, green for oxygen, purple for carbon and yellow for sulfur.

From Figure 15, it was observed that nickel and oxygen account for a substantial portion of the millerite surface. Interestingly, the feed nickel content was less than what was detected at pH 9. A higher sulfur and oxygen content was also observed in the feed. It can be seen that millerite has slight oxidation on the surface even for the freshly prepared feed sample. It is difficult to prevent the oxidation of millerite because it is very sensitive to air. Legrand et al. showed that even fracturing millerite in his XPS vacuum chamber, it still detected the presence of oxygen on the millerite. [46]

The nickel scans for the feed, pH 9 and pH 12 are seen in Figure 18, Figure 19, and Figure 20, respectively. A summary of all the nickel narrow scans can be found in Figure 21. The references are listed in Table 5 for the deconvolution of the XPS results.

From plant conditioned XPS narrow scans, it can be seen that the concentration of nickel sulphides decreased when the millerite was conditioned in solution. The amount of NiS on the surface of the millerite in the feed was found to be 25%. This decreased to 22 at pH 9 and then to 14 at pH 12. This is depicted by the decrease in peak height detected at 853.1 eV. The decrease in surface nickel sulphides can be mainly attributed to an increase in the nickel hydroxide and nickel oxide formation on the surface represented by binding energies at 855.8 eV and 854.2 eV, respectively. The surface of the feed sample was already mostly covered by $Ni(OH)_2$ at 35% but the concentration of $Ni(OH)_2$ increased further with higher pH. The surface coverage of $Ni(OH)_2$ at pH 12 accounts for almost half of the nickel detected at 45%.

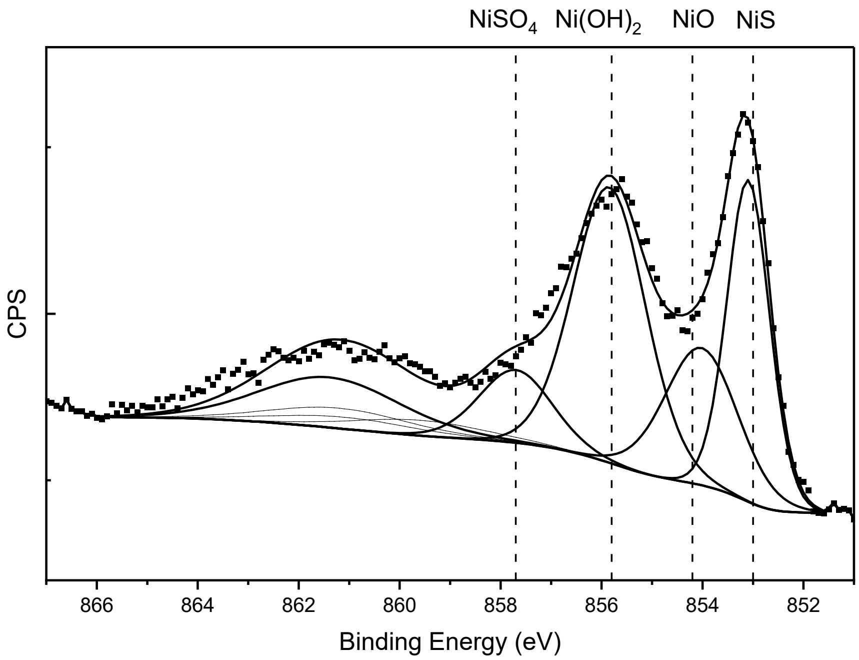

Figure 18. Nickel XPS narrow scan of millerite surface for the feed sample. The dotted lines are representative of the binding energies for NiSO$_4$, Ni(OH)$_2$, NiO and NiS from left to right.

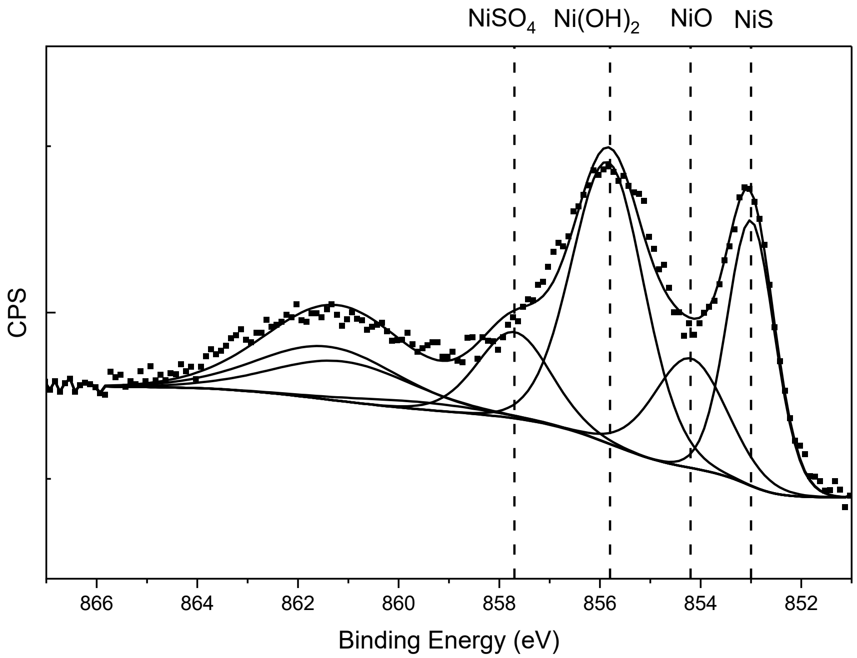

Figure 19. Nickel XPS scan of millerite surface for pH 9. The dotted lines are representative of the binding energies for NiSO$_4$, Ni(OH)$_2$, NiO and NiS from left to right.

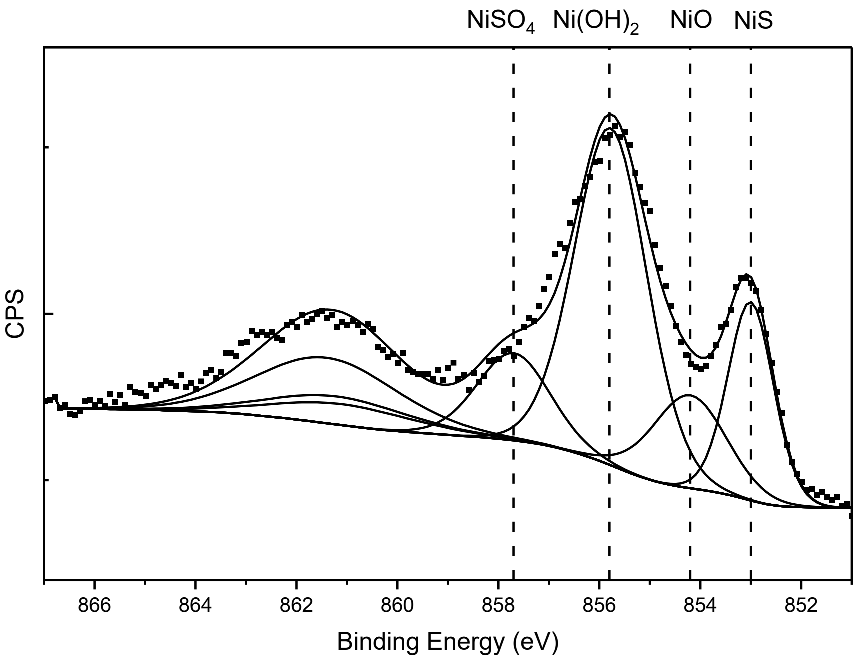

Figure 20. Nickel XPS scan of millerite surface for pH 12. The dotted lines are representative of the binding energies for NiSO₄, Ni(OH)₂, NiO and NiS from left to right.

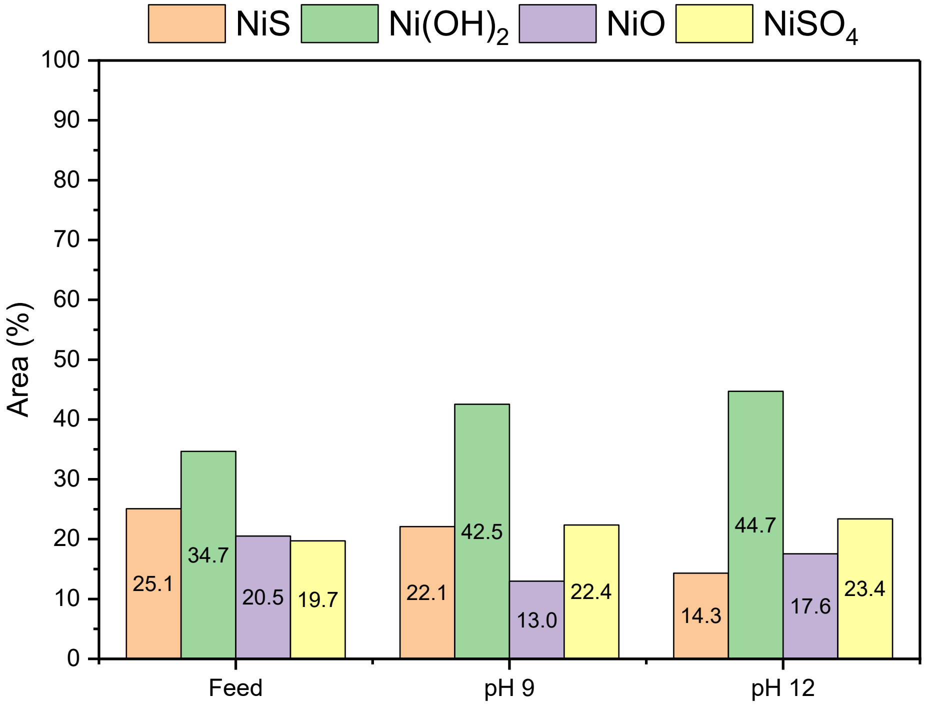

Figure 21. Summary of nickel XPS surface species for feed, pH 9 and pH 12. The colors represent: orange for NiS, green for Ni(OH)₂, purple for NiO and yellow for NiSO₄.

Table 5. XPS binding energy identification and references for nickel species

Nickel	Binding Energy	FWHM	Source
NiS	853.1	1.1	Legrand et al.
NiS - Satellite	859.7	3.2	Legrand et al.
Ni(OH)2	855.8	1.6	Legrand et al.
Ni(OH)2 - Satellite	861	3.2	Legrand et al.
NiSO4	856.7	1.6	Legrand et al.
NiSO4 - Satellite	862.3	3.2	Legrand et al.
NiO	853.7		Nesbitt 2000
NiO - Satellite	860.7		Nesbitt 2000

The large decrease of nickel sulphides on the surface of millerite at pH 12 as well as the large surface coverage of $Ni(OH)_2$ could be the reason for the exhibited millerite flotation behavior. Nickel hydroxide is known to be hydrophilic, causing the surface of millerite to be less attracted to air bubbles. Surface sulfur imparts hydrophobic properties, but concentrations are low at high pH. The increase of nickel hydroxide on the surface at pH 12 is probably caused by the precipitation of hydroxide ions in solution onto the surface, creating a passivation layer. As a result, this passivation layer covers the nickel sulfides on the surface, thereby causing the surface to become more hydrophilic. The nickel sulphate concentration on the surface remains relatively the same on the feed surface and at pH 9. There is a slight increase in sulphate concentration at pH 12 which accounts to about 23.4% of the surface nickel. Since sulphates on the surface do not change significantly at different pH, this means that sulphates do not contribute greatly to the flotation of millerite. This is to be expected as the formation of sulphates takes much longer than the time flotations are run. [38]

The nickel oxides on the surface had the highest concentration in the feed sample and actually decreased when it was conditioned at pH 9 and 12. This is probably due to the shift from nickel oxides to nickel hydroxides since the sulfate concentration did not increase. The main contribution to the flotation patterns seen in millerite can therefore be attributed to the hydroxide ions on the surface of millerite.

The sulfur scans for the three conditions can be seen in Figure 22, Figure 23, and Figure 24. The black lines represent the main peak for each chemical species and the gray peaks represent their corresponding doublets. Deconvolution for sulfur species was based on the work done by Legrand et al. 1997. The doublets were calculated based on the binding energy of the main peak by adding 1.18 eV. [63] The NiS and polysulfides in the sulfur scans are beneficial for millerite flotation due to their hydrophobic nature, whereas the oxidation product $NiSO_4$ is detrimental for millerite flotation. From the results, the sulfur peaks do not exhibit very noticeable differences between the different experimental conditions. By looking at Figure 25, it can be seen that if surface NiS and polysulfides are combined, they account for 90% of the sulfur species existing on the millerite surface at all conditions. This means that sulphides do not play a significant role in the flotation behavior of millerite in alkaline conditions. Although sulphide flotation depends on the oxidation of sulphides, millerite flotation behavior is more dependent on its nickel ions.

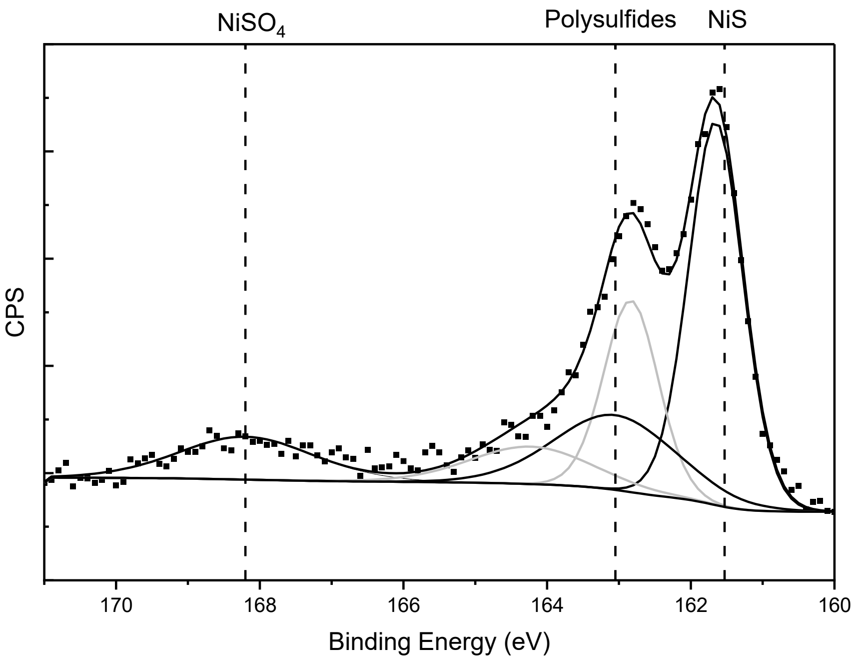

Figure 22. Sulfur XPS narrow scan for millerite for feed sample. The dotted lines are representative of the binding energies for NiSO₄, polysulfides and NiS. The lines in grey are the spin-orbit doublets.

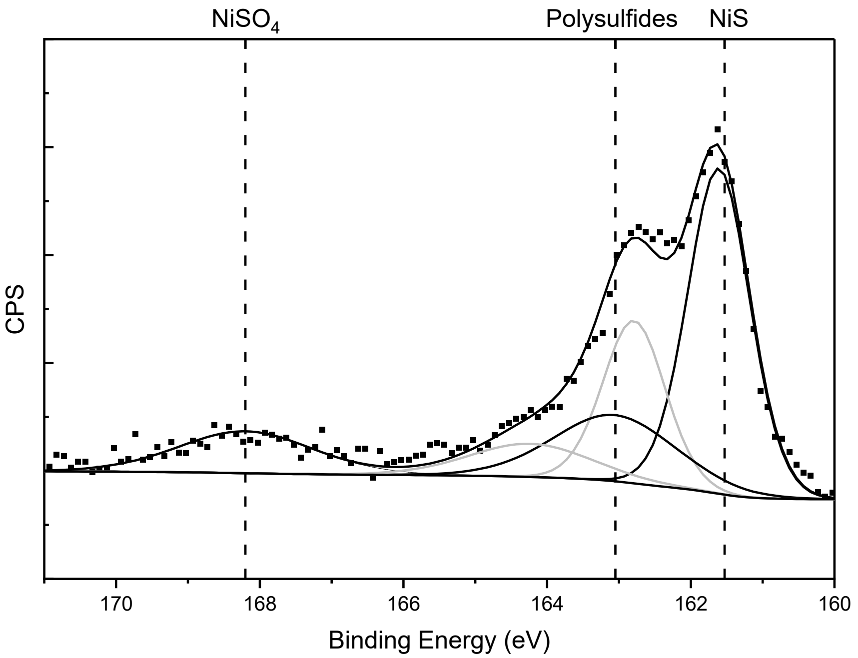

Figure 23. Sulfur XPS narrow scan for millerite surface for pH 9. The dotted lines are representative of the binding energies for NiSO₄, polysulfides and NiS. The lines in grey are the spin-orbit doublets.

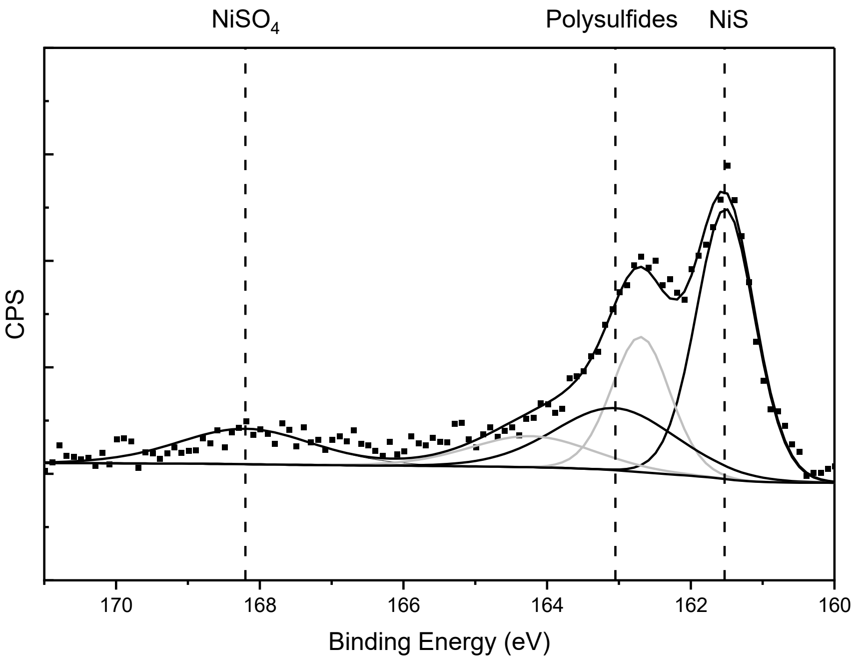

Figure 24. Sulfur XPS narrow scan for millerite surface for pH 12. The dotted lines are representative of the binding energies for NiSO₄, polysulfides and NiS. The lines in grey are the spin-orbit doublets.

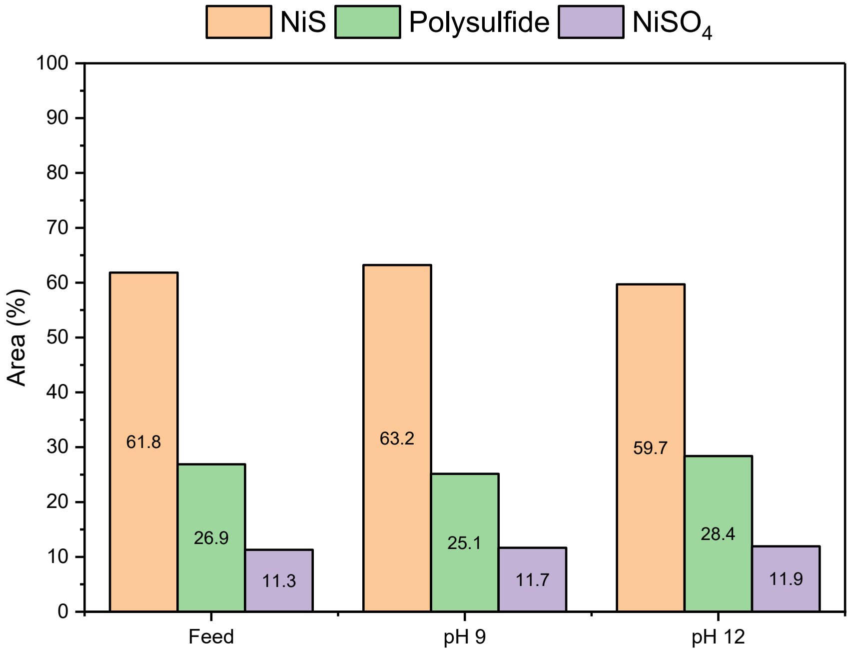

Figure 25. Summary of sulfur XPS surface species for feed, pH 9 and pH 12 The colors represent: orange for NiS, green for polysulfide, purple for NiSO₄.

There appears to be either dissolution of surface sulfur or possible precipitation of $Ni(OH)_2$ occurring at pH 9, which explains the lower nickel and higher sulfur content in the feed seen in Figure 15. From the scans, it can be seen that millerite flotation depends primarily on the behavior of nickel ions and is not heavily impacted by sulfur ions.

4.3 Cyclic Voltammetry Results for Millerite

To get a better understanding of how millerite is affected by different oxidizing and reducing potentials, cyclic voltammetry (CV) experiments were conducted. Scans were performed in the oxidizing and reducing directions at pH 9 and pH 12, provided in Figure 26 and Figure 27, respectively. The black lines represent scans done in the positive oxidizing direction while the red lines represent scans beginning from the reducing negative direction. Experiments were also done to study the effect of a rotational electrode versus a stationary electrode represented by the solid and dotted lines, respectively.

Figure 26 shows that the electrode spinning at 2000 RPM had a higher oxidative peak than the stationary electrode. This means that rotating the electrode caused the surface to become more susceptible to oxidation. This could be due to the breaking of an oxidation passivation layer that was formed on the surface of the millerite when it was not in motion. The passivation layer can be attributed to the precipitation of $Ni(OH)_2$ that was detected by the XPS scans earlier or by the oxidation of sulfur to sulfate. The peak plateaus for both instances when no additional oxidation occurs. This effect is not seen in Figure 27 where scans in the oxidating direction appear similar when comparing the stationary electrode to the moving electrode. This is possibly due to the high concentration of hydroxide ions already present in the solution at pH 12 creating a stable passivation layer that is unaffected by rotation. The direction the CV was scanned did not affect the surface species present on the millerite surface for both pH 9 and pH 12. The trend for multiple cycle scans of the millerite electrode surface remained the same and hence surface products did not change.

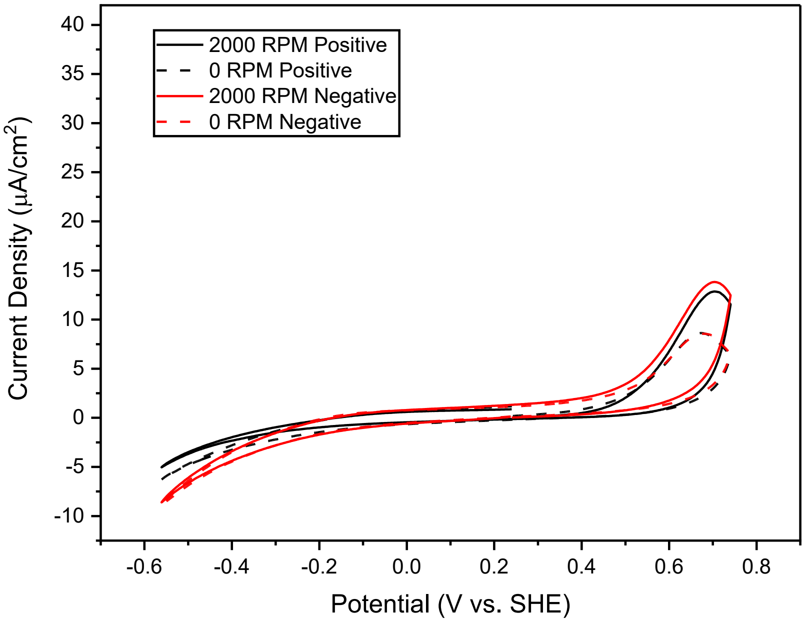

Figure 26. Cyclic voltammetry scan for millerite electrode at pH 9 in buffer solution at rotating (solid lines) and stationary conditions (dotted lines). Scans completed in the positive oxidating and negative reducing directions are shown in red and black, respectively.

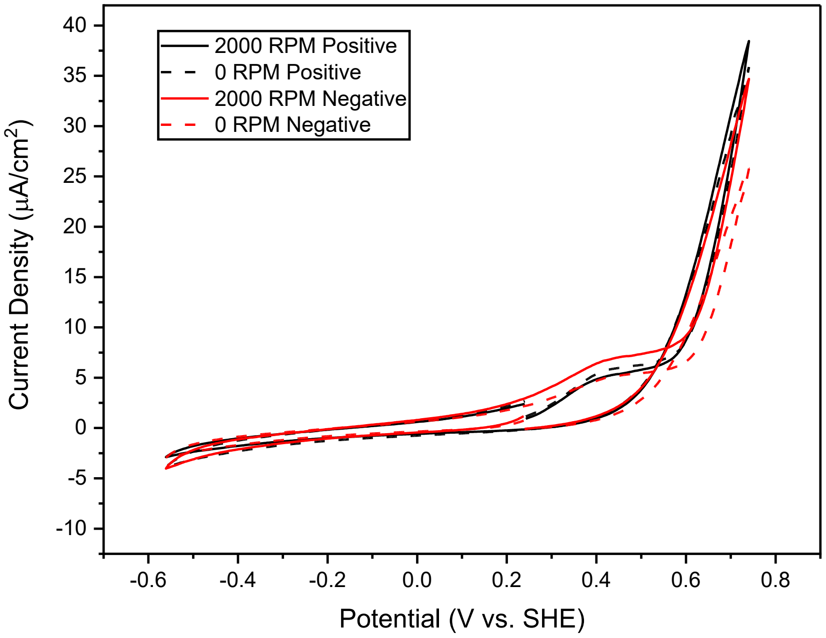

Figure 27. Cyclic voltammetry for millerite at pH 12 at rotating (solid lines) and stationary conditions (dotted lines). Scans completed in the positive oxidating and negative reducing directions are shown in red and black, respectively.

Calculations were performed to predict the possible species existing on the millerite electrode. They were calculated based on the Gibbs free energy given by Gamsjäger et al. 2005 [61] and then combined with the Nernst equation, assuming an ion concentration of 1 M. The dissolution of millerite into Ni^{2+} and the oxidation to sulfur reaction begins at 0.236 V and is not pH dependent. This value decreases if the concentration of Ni^{2+} is less than 1 M. The reaction of NiS with water to produce $Ni(OH)_2$ starts to occur at 0.0313 for pH 9 and -0.146 V for pH 12. This trend is consistent with the flotation pulp potentials that were observed and is consistent with the speciation diagram found in Figure 6. Due to the abundance of possible sulfide species existing, it is hard to predict the exact reasons for the peaks that are observed in the cyclic voltammetry graphs. One possible explanation for the peak that is observed at 0.4 V for pH 9 and for the peak at 0.6 V at pH 12 could be the formation of sulfates on the surface given by Equation 4.1.

$$S^0 + 4H_2O \longrightarrow SO_4^{2-} + 8H^+ + 6e^- \qquad \text{Equation 4.1}$$

Calculations done using the Nernst Equation (3.1) and by assuming 1 M concentration for SO_4^{2-}, the calculated E_{cell} was found to be 0.357 V for pH 9 and 0.594 V for pH 12. The additional oxidation peak observed at 0.2 V at pH 12 could not be determined and would need further surface analysis to accurately identify the surface species.

4.4 Contact Angle Measurements for Millerite

The captive bubble measurements shown in Figure 28 for millerite were performed using Biolin Scientific Attention Theta tensiometer and the results are given in Figure 29. The contact angle measurements were used to confirm the results seen in the single mineral flotation data. The contact angle at pH 9 was found to be 37° and at pH 12, it was 15°. The higher contact angle seen at pH 9 means that the surface is more hydrophobic, resulting in a higher affinity for bubble attachment. The lower contact angle at pH 12 means the surface is very hydrophilic resulting in less bubble attachment. The contact angle measurements help explaining the flotation recoveries that were observed. The results are further supplemented by the XPS data that conclude millerite surfaces are greatly affected by hydroxides, which are known to be hydrophilic.

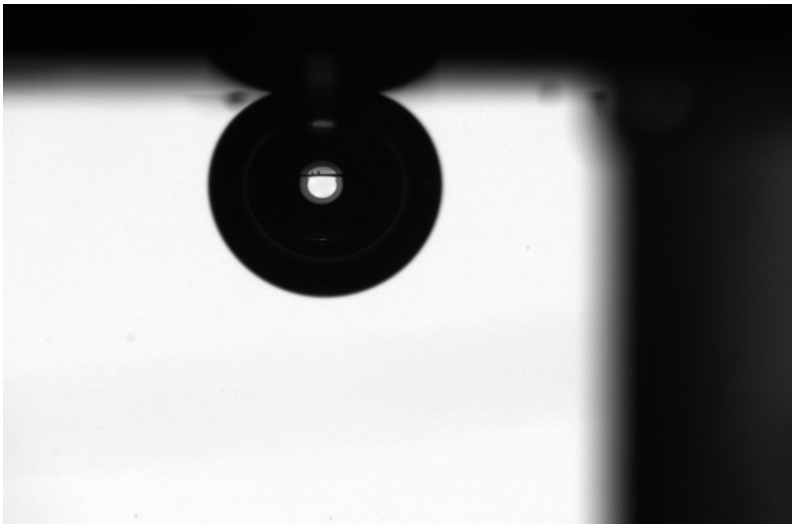

Figure 28. Captive bubble contact angle experiment for millerite electrode

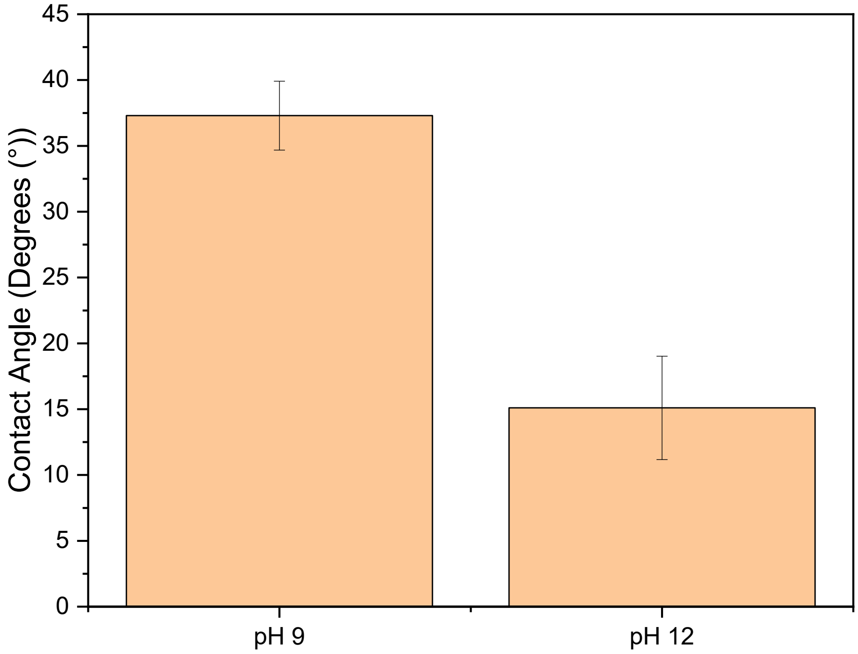

Figure 29. Contact angle measurements using captive bubble for millerite at pH 9 and pH 12

Chapter 5: Galvanic Interaction

5.1 Single Mineral Flotation of Chalcopyrite and XPS

To establish a baseline for the flotation behaviour of chalcopyrite without the effect of millerite interactions, micro-flotations of chalcopyrite were conducted. The recovery results for chalcopyrite are presented in Figure 30. The flotation results for chalcopyrite were similar for all the pH tested and did not seem to be affected by the pulp potential. The flotation recovery was found to be around 80-85% and matched results found in the literature. [38], [64], [65]

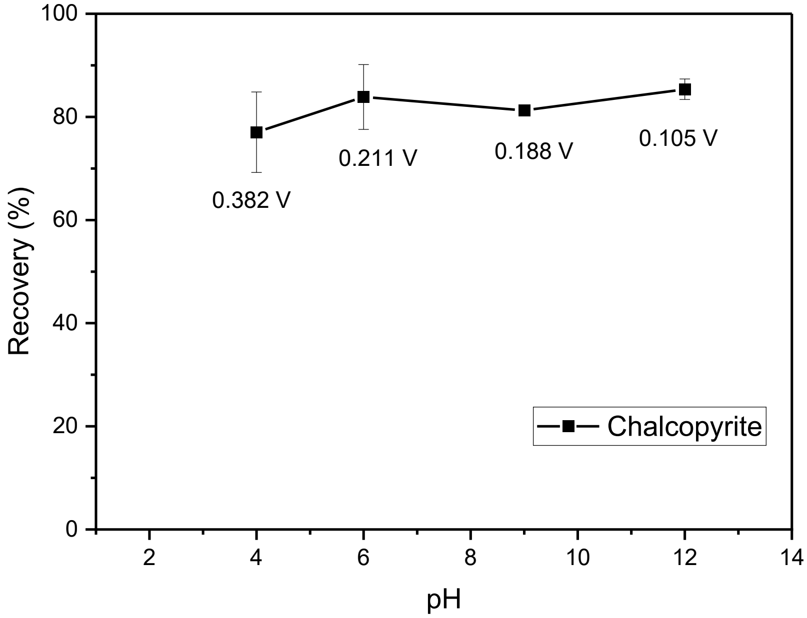

Figure 30. Collectorless single mineral flotation of chalcopyrite at pH 4, 6, 9, and 12 with pulp potential measured in SHE.

An additional sweep of the chalcopyrite powder surface was conducted by using XPS to study how the surface changes at different pH. From the overall scan in Figure 31, it can be seen that results at pH 9 and 12 have relatively the same intensity. The oxygen content accounts for a small percentage of the surface, which is mainly composed of copper species. The results show that chalcopyrite is less likely to get oxidized when compared to the millerite single mineral flotation results shown before. Surprisingly, the signal for iron is not that strong in chalcopyrite. The copper scans for the chalcopyrite surface can be seen in Figure 32 and the summary of the copper species distribution is given in Figure 33. From the results, it can be seen that the ratio of copper species at pH 9 and pH 12 are very similar.

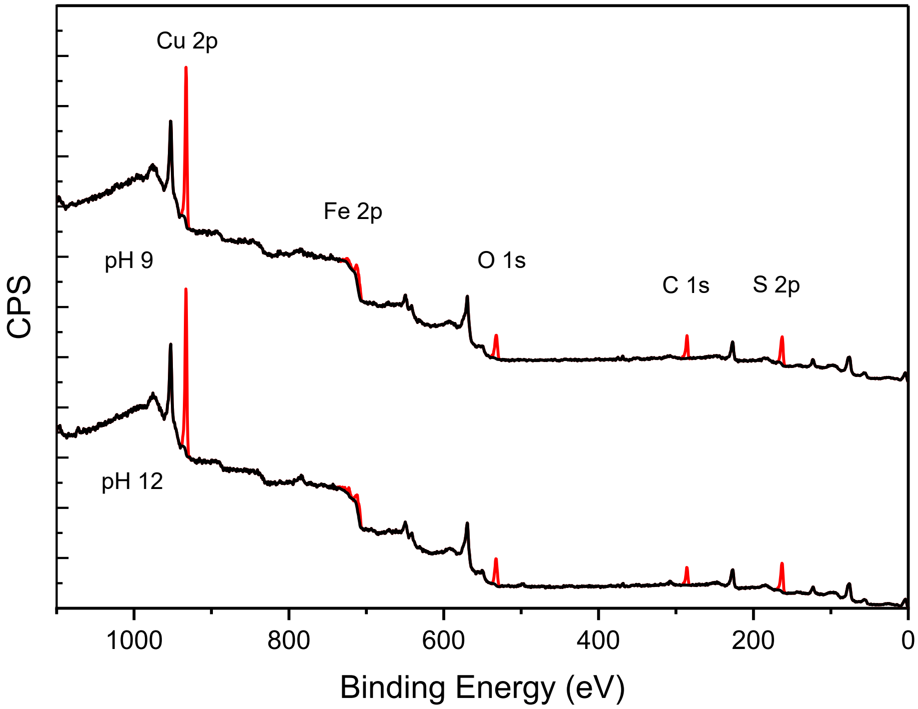

Figure 31. Survey scans for chalcopyrite powdered samples conditioned at pH 9 and pH 12. The black lines are representative of the background and the red lines are the peaks for Cu 2p, Fe 2p, O 1s, C 1s and S 2p from left to right.

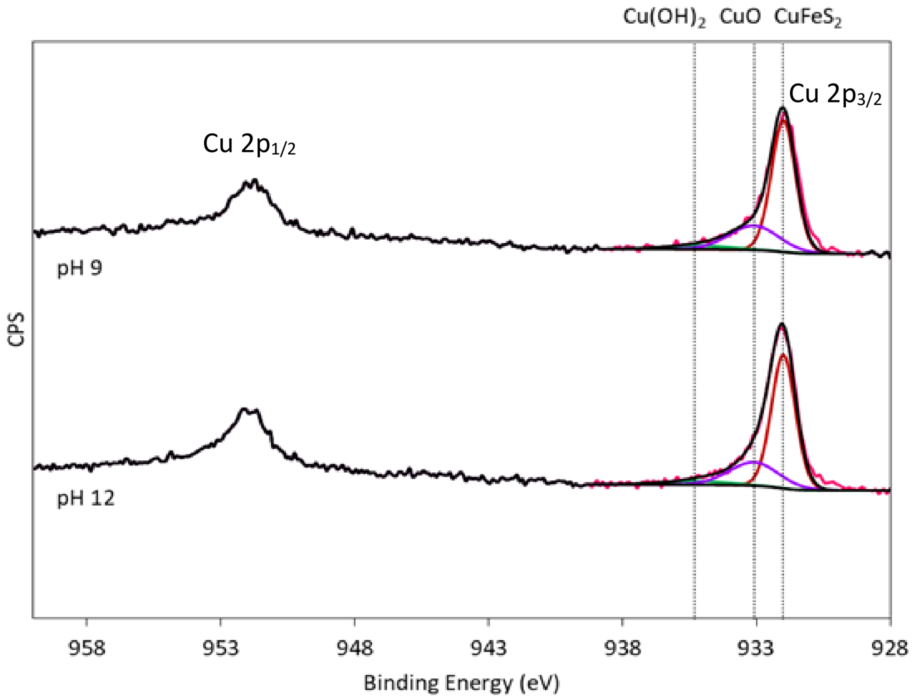

Figure 32. Copper XPS narrow scans of chalcopyrite surface at pH 9 and pH 12. The dotted lines are representative of the binding energies for $Cu(OH)_2$, CuO, and $CuFeS_2$ from left to right.

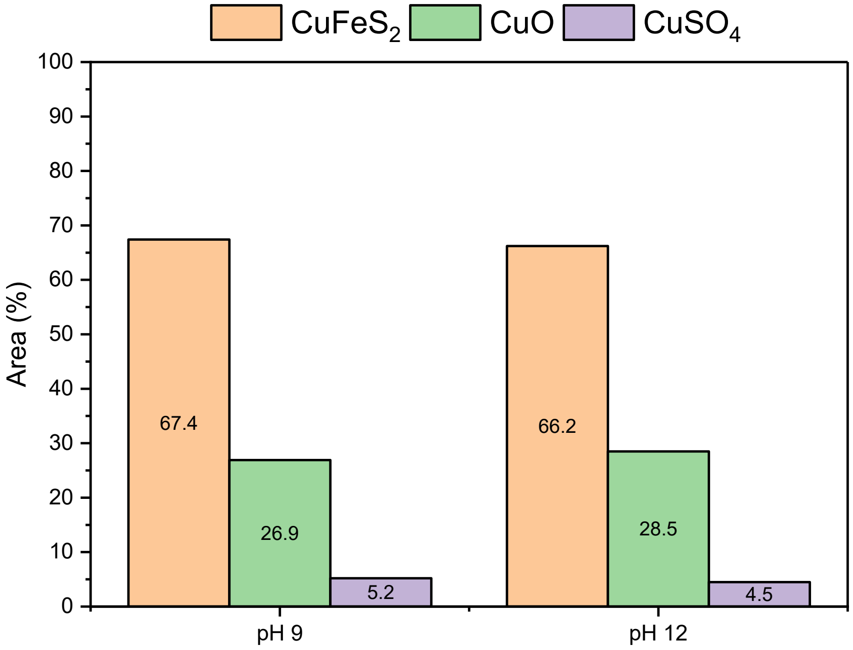

Figure 33. Summary of the copper XPS surface species for chalcopyrite at pH 9 and pH 12. The colors represent: orange for $CuFeS_2$, green for CuO, and purple for $Cu(OH)_2$.

5.2 Mixed Flotation of Millerite and Chalcopyrite

The experimental results for mixed mineral flotation can be seen in Figure 34 and Figure 35 for millerite and chalcopyrite, respectively. The mixed millerite recovery mirrored the results from the single mineral recovery. The trend was the same with only a minor increase in flotation recovery of millerite at pH 12 but this could possibly be due to experimental error. However, the chalcopyrite showed slight depression when compared to its single mineral flotation results. The recovery dropped from 85.4% to 69.3%. This is uncommon as flotation recovery of chalcopyrite is consistently high. Since the only difference is the presence of millerite, this means that millerite has a depressive effect on chalcopyrite at pH 12. This can be attributed due to the precipitation of nickel hydroxides onto the chalcopyrite surface as it is shown from the XPS analysis of the millerite surface that the majority of the surface is covered by $Ni(OH)_2$. This effect is not observed at pH 9 because the pH is not high enough for the formation of $Ni(OH)_2$ in solution as observed from Figure 6's speciation diagram. In addition, Liu et al. (2021) [54] observed similar depression behaviors to pyrite and chalcopyrite as cathodes when floated with pyrrhotite and pentlandite as a result of galvanic interaction.

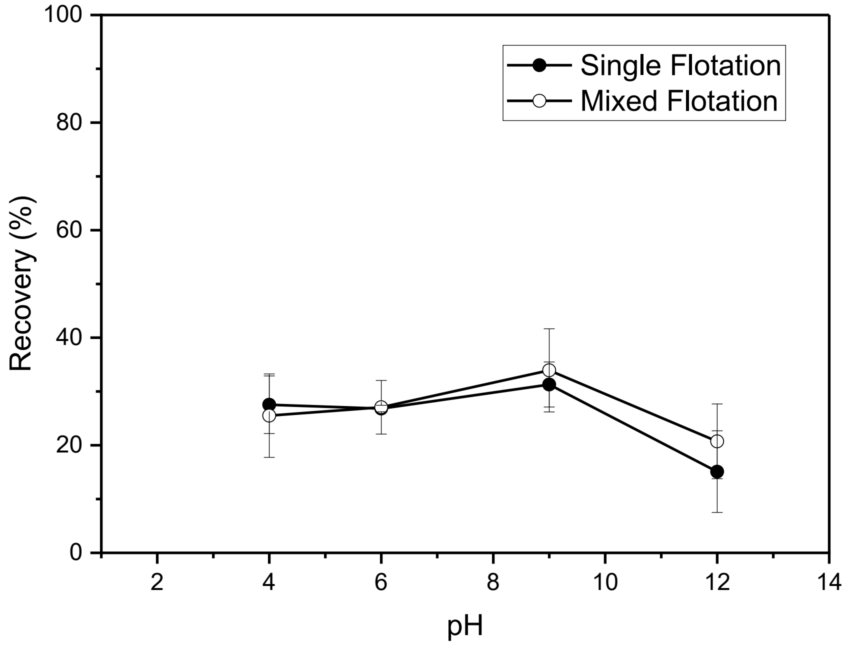

Figure 34. Millerite recovery for mixed mineral flotation of millerite with chalcopyrite at pH 4, 6, 9, and 12. The mixed flotation results are shown by the unfilled circles and the filled circles are results from single mineral flotation.

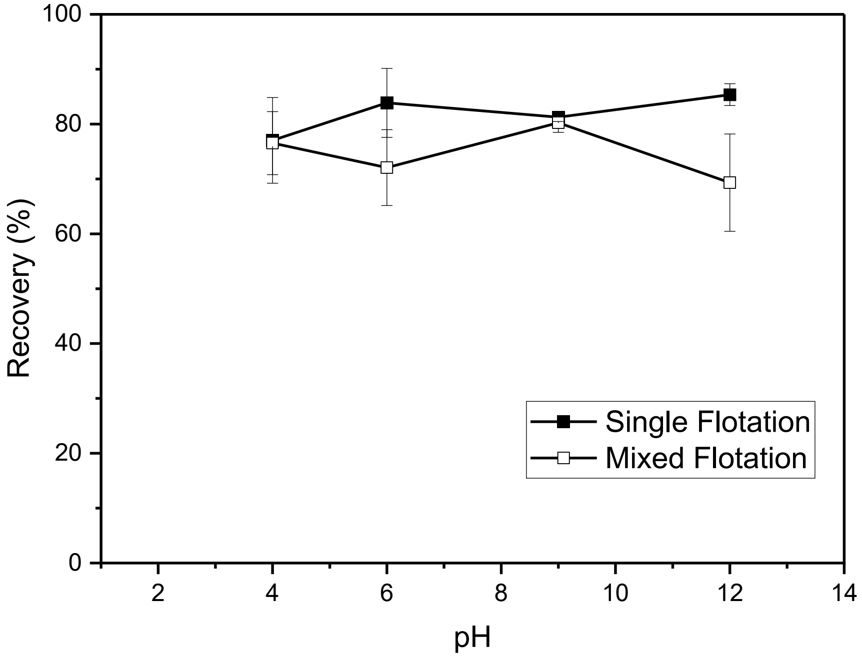

Figure 35. Chalcopyrite recovery in mixed mineral flotation of millerite with chalcopyrite at pH 4, 6, 9, and 12. The mixed flotation results are shown by the unfilled squares and the filled squares are results from single mineral flotation.

5.3 Rest Potential Measurements of Chalcopyrite and Millerite

One way to confirm whether millerite and chalcopyrite affect each other electrochemically is by measuring the rest potential. If rest potentials are similar, then the cause for the depression of chalcopyrite at pH 12 is not due to electrochemical differences. However, if the two rest potentials are greatly different then galvanic interaction will impact flotation behavior. [66] It is important to measure the rest potentials of chalcopyrite and millerite to determine which mineral acts as the anode and the other as the cathode. From the results in Figure 36, it can be concluded that chalcopyrite is the cathode and millerite acts as the anode. From the graph, it shows the surface achieved equilibrium after being conditioned for 5 minutes. The two rest potentials averaged 0.163 V for chalcopyrite and 0.038 V for millerite. The difference in the two rest potentials is 0.125 V which means that galvanic interaction should influence flotation recovery. The chalcopyrite would undergo reduction and increased oxidation of millerite would occur.

The behavior of chalcopyrite acting as the anode has been rigorously studied in relation to other sulfides. [38, 53, 67] However, information on chalcopyrite acting as the cathode are not as clear. From the collectorless flotation results, it is surprising that chalcopyrite was depressed. An in-depth study of the effect of millerite oxidation on chalcopyrite was conducted to understand the flotation behavior.

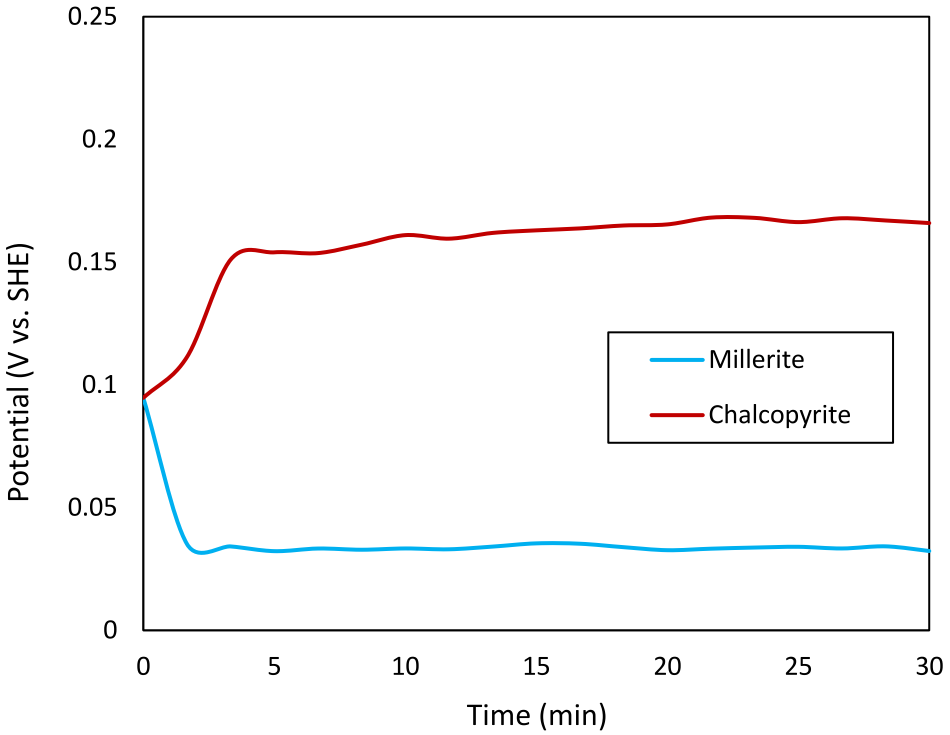

Figure 36. Rest potential measurements of millerite and chalcopyrite at pH 12 without the addition of collectors. The blue and red lines represent millerite and chalcopyrite, respectively.

5.4 Millerite and Chalcopyrite Dissolution

Samples were collected from millerite and chalcopyrite in pH adjusted solution and then analyzed with inductively coupled plasma mass spectrometry (ICP-MS). This provides important data on the metal dissolution on both minerals. The results can be seen in Table 6. The millerite at pH 9 releases 2.5 ppm of Ni ions but this quickly drops to 0.12 ppm at pH 12. This is most likely due to the precipitation of $Ni(OH)_2$ at pH 12 and less stable formation at pH 9. There are trace amounts of Cu and Fe ions in the millerite dissolution ICP due to impurities. Chalcopyrite did not exhibit high dissolution in solution, with very few ions detected.

At pH 9 mixed conditions, the presence of chalcopyrite helped to increase the dissolution of nickel ions from millerite. In single mineral conditions, millerite only released 2.5 ppm but this increased to 5.98 ppm in mixed conditions. This means that the presence of chalcopyrite caused millerite to release more nickel ions. This is expected from the rest potential results because millerite in the presence of chalcopyrite is further oxidized due to the potential difference. The oxidation of millerite begins with the release of nickel ions (see Equation 2.5), supporting the results of this work. Due to the high pH and the formation of hydroxides, nickel dissolution is not seen at pH 12 even in mixed conditions. From these results, it is not possible to conclude whether the nickel ions transferred onto the chalcopyrite causing the depression in recovery or if it has passivated onto the millerite.

Table 6. ICP results for single and mixed mineral dissolution

Condition	Element	Solution Concentration (ppm)
pH 9 NiS	Ni	2.5
	Cu	0.01
	Fe	0.01
pH 12 NiS	Ni	0.12
	Cu	0.03
	Fe	0.04
pH 9 Cp	Ni	0
	Cu	0
	Fe	0.01
pH 12 Cp	Ni	0
	Cu	0.01
	Fe	0.04
pH 9 Mixed	Ni	5.98
	Cu	0
	Fe	0
pH 12 Mixed	Ni	0
	Cu	0.01
	Fe	0.03

5.5 Nickel Ion Effects on Chalcopyrite and EDTA Extraction

Due to the stability of chalcopyrite recovery at all pH levels except in the presence of NiS, experiments were done to confirm whether chalcopyrite recovery could be affected by Ni ions. In order to investigate the cause for chalcopyrite depression during mixed flotation at pH

12, nickel sulphate was added to chalcopyrite single mineral flotation to see its effects. Dissolved $NiSO_4$ solution was immediately added after the minerals were immersed in solution. The results in Figure 37 show that even a small concentration of $NiSO_4$ (1 ppm) can dramatically affect the flotation recovery of collectorless chalcopyrite. The presence of Ni species on chalcopyrite is sufficient to decrease its recovery.

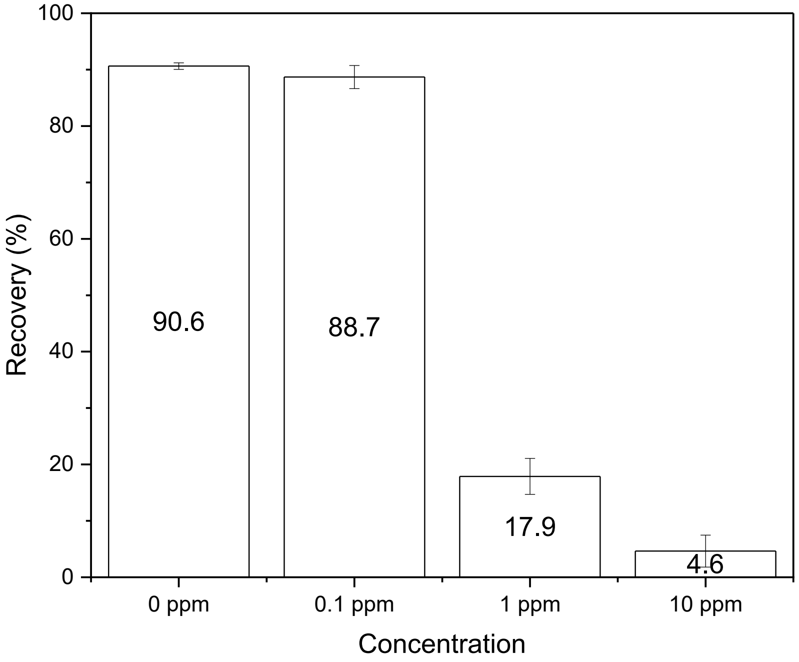

Figure 37. Collectorless recovery of chalcopyrite as a function of $NiSO_4$ concentration at pH 12

To confirm that the presence of nickel oxidative products, ethylenediaminetetraacetic acid (EDTA) extraction was used on a chalcopyrite electrode conditioned with millerite powder. Analyses using ICP-MS showed that the concentrations were 0.017 ppm for nickel, 0.015 ppm for iron and 0.115 ppm for copper. Although the concentration of nickel is low, it nevertheless confirms that there is migration of nickel species from millerite. Additionally, the surface area in flotation experiments would be greater than the exposed surface of the electrode and hence more transfer is expected.

5.6 XPS Results for Mixed Mineral Samples

Mixed powders were used in the first attempt to identify the presence of millerite on chalcopyrite as a result of galvanic interaction. 38-75 µm chalcopyrite was mixed with less than 38 µm fraction of millerite and then conditioned at pH 12. Using PHI XPS, chalcopyrite particles were identified based on its size and narrow scans were used to confirm. The narrow scans were performed for 1-1 as seen in Figure 38. From the nickel narrow scan on the chalcopyrite particle, as seen in Figure 39, it can be determined that there is a slight presence of nickel species on the chalcopyrite. The narrow scan for nickel was performed 12 times but from the results, the signal for nickel on the chalcopyrite was very weak. Deconvolution of nickel species could not be performed due to fluctuations, but the presence of nickel on chalcopyrite can be confirmed.

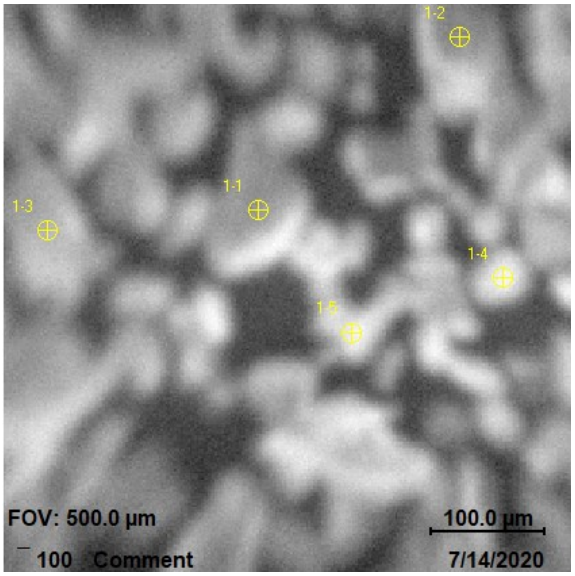

Figure 38. PHI XPS imaging of millerite powder conditioned with chalcopyrite powder at pH 12.

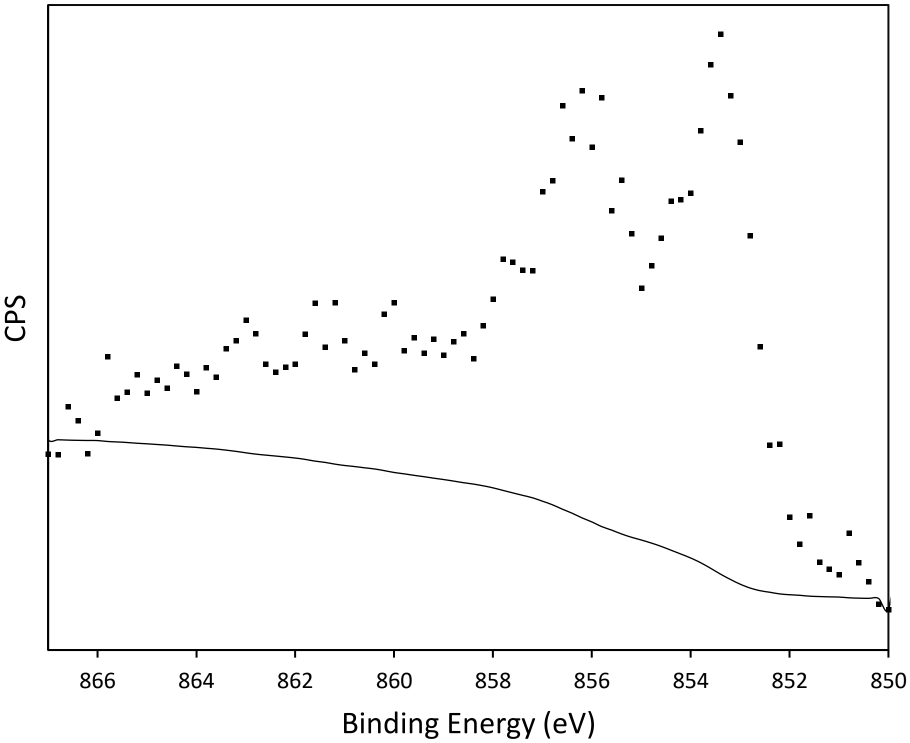

Figure 39. XPS narrow scan of nickel on chalcopyrite powder conditioned at pH 12 with millerite.

A more direct approach was used by conditioning a chalcopyrite electrode with millerite powders. The survey scan of the chalcopyrite surface can be seen in Figure 40. Figure 41 and Figure 42 show the surface that was used for the overall scan. The elements that are further studied using the narrow scan are shown in red. From Figure 37, there is a noticeable peak at 850 eV to 860 eV, representative of nickel detected when the electrode is conditioned with NiS powder. In the baseline scan, there is no detectable nickel on the surface. This means that during conditioning, nickel species are transferred onto the chalcopyrite.

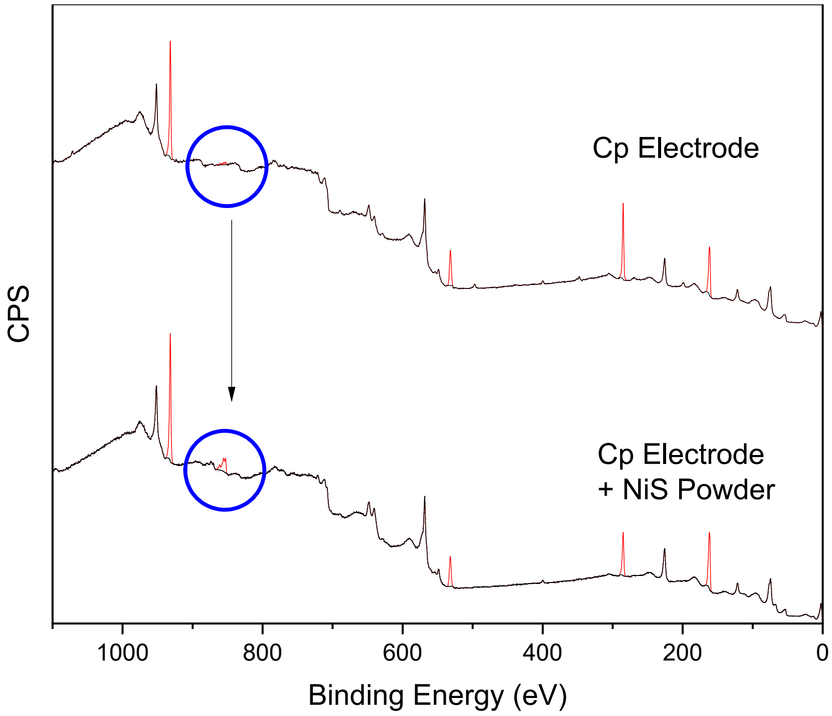

Figure 40. Survey scan of chalcopyrite electrode at conditioned pH 12 with and without millerite powders. When the chalcopyrite electrode is conditioned with NiS powder, there is a peak at 850-860 eV that is representative of nickel species.

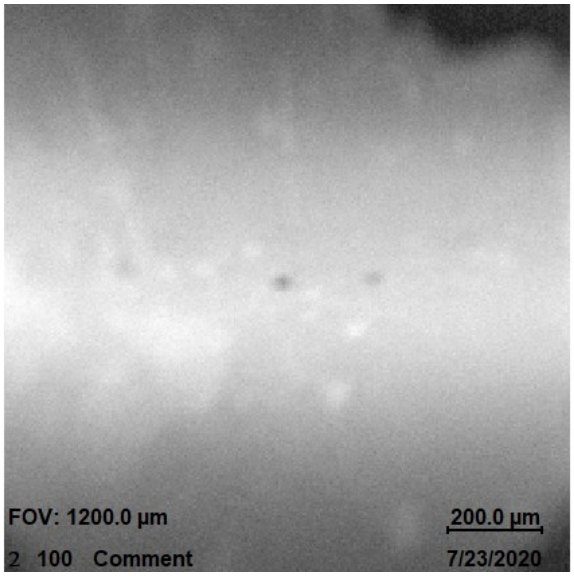

Figure 41. PHI XPS surface image of chalcopyrite electrode.

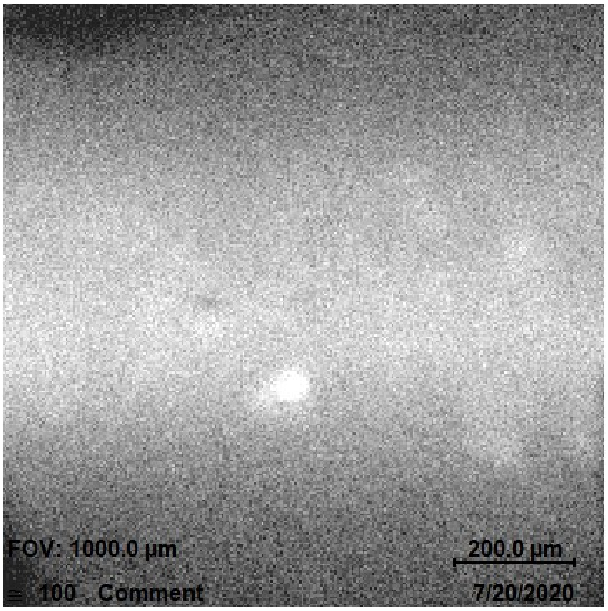

Figure 42. PHI XPS surface image of chalcopyrite electrode conditioned with millerite powder.

The deconvolution of nickel species on the surface of the chalcopyrite cathode can be seen in Figure 43 following methods used in analyzing the millerite surface shown before. The main contribution to the surface nickel seems to be caused by NiS followed by $Ni(OH)_2$ as seen in Figure 44. The only difference between the single mineral flotation of chalcopyrite at pH 12 and the mixed flotation experiment was the presence of millerite, and from the surface scans the presence of nickel products on chalcopyrite was confirmed. Therefore, it is plausible to conclude that millerite has a depressive effect on chalcopyrite under collectorless conditions.

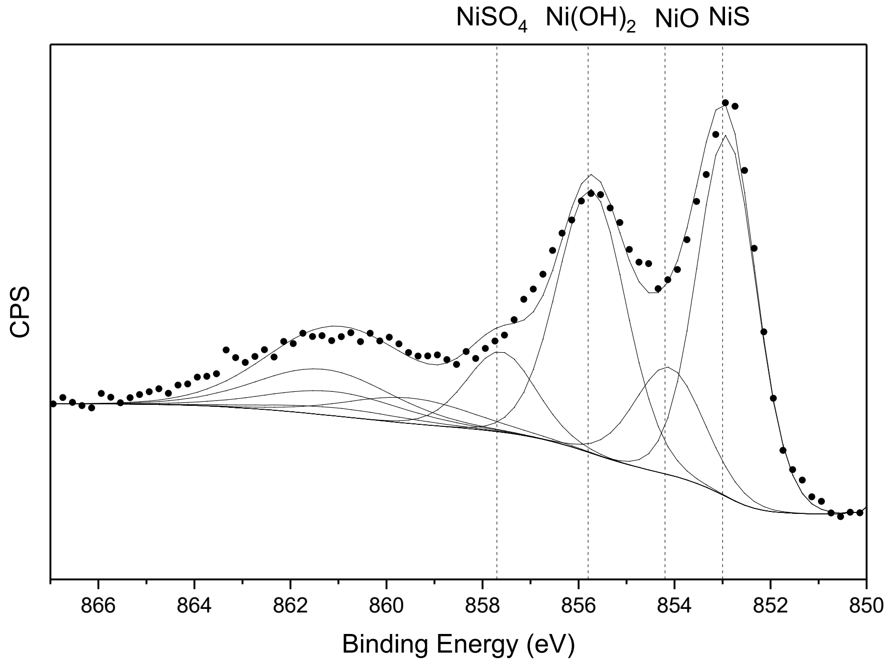

Figure 43. PHI XPS narrow scan of nickel on chalcopyrite electrode at pH 12. The dotted lines are representative of the binding energies for $NiSO_4$, $Ni(OH)_2$, NiO and NiS from left to right.

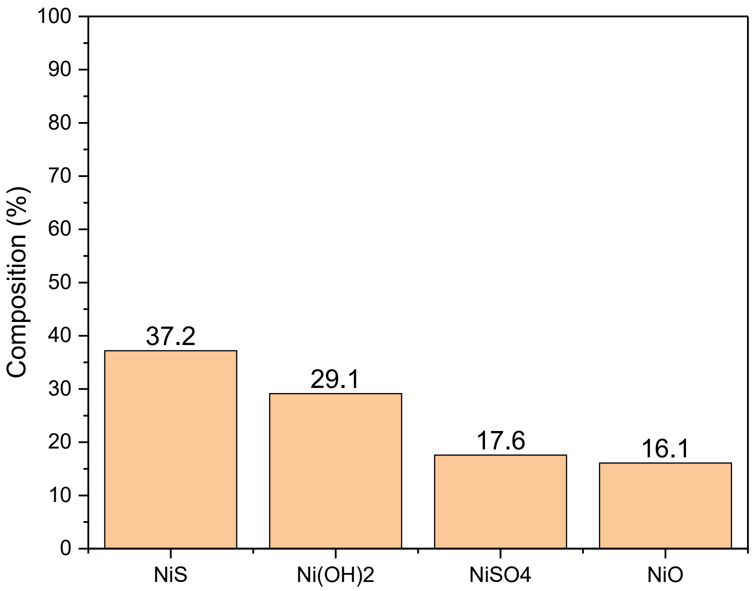

Figure 44. Nickel surface species distribution on chalcopyrite electrode that has been conditioned with millerite powder.

5.7 Galvanic Interaction in the Presence of Xanthate

There is evidence to suggest that galvanic interactions exist between millerite and chalcopyrite under collectorless conditions. This section investigates how millerite and chalcopyrite galvanic interaction changes when xanthate collector is added.

From Figure 45, the equilibrium rest potential for chalcopyrite and millerite is very similar when potassium ethylxanthate (KEX) collector is added. There is a difference of 8.5 mV at pH 9 and 2 mV at pH 12. This means that due to the closeness in potential, galvanic interaction would not be apparent if there is already xanthate pre-adsorbed onto the surface. This is further supported by the flotation experiments presented in Figure 46. From this graph, it can be seen that even when the two minerals are conditioned together prior to the addition of xanthate, it would still have significant recovery after the addition of KEX. The collector increases the recovery similar to levels observed when the minerals are conditioned with the collector added in together. This means that galvanic interactions are too weak in the presence of collectors and would not greatly affect flotation behaviours.

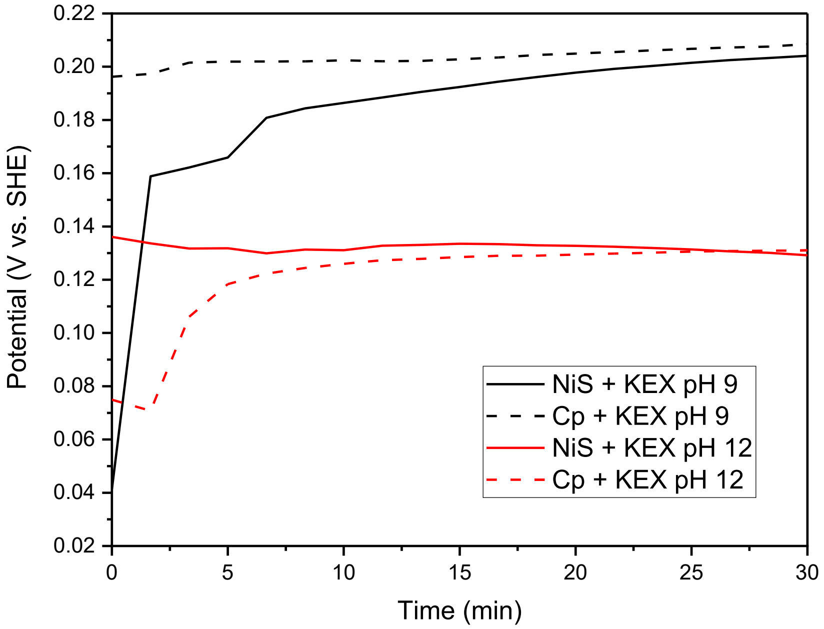

Figure 45. Rest potentials of millerite and chalcopyrite at pH 9 (black lines) and 12 (red lines) with the addition of KEX. The solid lines represent rest potentials of millerite and dotted lines represent chalcopyrite.

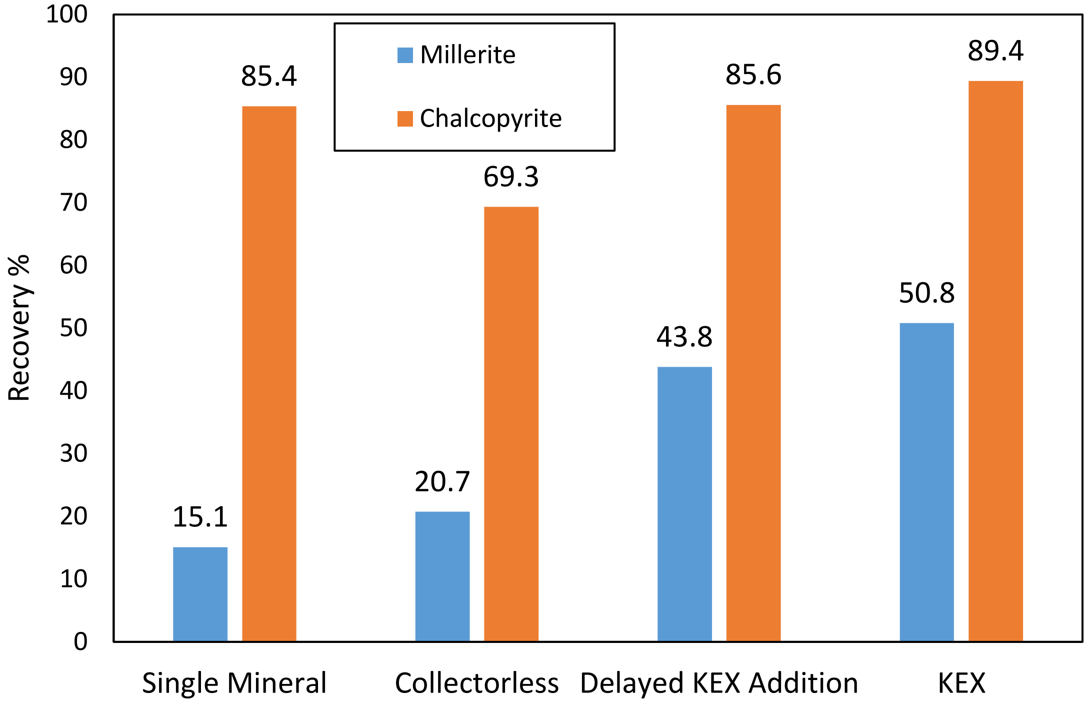

Figure 46. Flotation experiments with the addition of KEX after a conditioning time of 5 minutes. Millerite and chalcopyrite are shown in blue and orange, respectively.

Chapter 6: Conclusions and Recommendations

6.1 Conclusion

The millerite flotation behaviour was studied by understanding the changes to its surface as it underwent oxidation. Millerite was found to be slightly floatable in acidic and low alkaline solutions, but recovery dropped when the pH was increased to 12. Through the use of XPS analysis, it was determined that at pH 12, 44% of the surface nickel could be attributed to $Ni(OH)_2$, which is hydrophilic. This explained why millerite recovery decreased at pH 12. From the XPS results, it was found that $NiSO_4$ did not play a huge role in millerite flotation since the surface area coverage did not change significantly. By looking at the cyclic voltammetry data, the surface species at each pH could be predicted. Additional changes to the surface as a result of oxidation and reduction could be observed.

It was found that the presence of millerite affected the flotation recovery of chalcopyrite under collectorless conditions. From the mixed flotation results, millerite flotation was determined to be relatively unaffected, while chalcopyrite recovery dropped at pH 12. Chalcopyrite is known for its consistently high flotation recovery and is surprising that millerite caused it to be depressed. By testing the rest potential of millerite and chalcopyrite, it was determined that chalcopyrite acted as a cathode and millerite acted as the anode. From the ICP results, it was determined that chalcopyrite induced oxidation of millerite, causing the additional release of nickel ions into solution. EDTA and ICP were used to confirm the presence of nickel species on chalcopyrite. Further analysis of the nickel species on the surface of chalcopyrite was conducted using PHI XPS. The presence of NiS and $Ni(OH)_2$ was confirmed, which explained why flotation recovery had decreased.

The galvanic interaction between chalcopyrite and millerite did not occur in the presence of xanthate due to changes in the rest potential. The difference in rest potential between the two minerals drastically decreased resulting in little to no galvanic interaction. Hence, galvanic interaction would only occur during collectorless mixed flotation for millerite and chalcopyrite.

With the knowledge of how millerite and chalcopyrite behave, Strathcona mill can implement the information found here to prevent the depression of chalcopyrite in the presence of millerite. In addition, by identifying the surface species responsible for millerite flotation behavior, targeted depression approaches can be developed, effectively separating millerite from chalcopyrite. This in turn ensures that the targeted nickel concentration in the copper concentrate remains low so that the penalty can be avoided.

6.2 Recommendations

Research on millerite is still not thoroughly completed with multiple questions that are still left unanswered. The main goal of understanding millerite flotation behavior is to ensure its depression in real industrial applications. The information provided in this thesis serves as a building block and additional research is needed to reach this goal.

The next step in fundamental understanding the millerite behaviour would be to investigate how collector affects the flotation of the two minerals, followed by development of depressants or physical methods to depress millerite. The study on the effect of grinding media on flotation of millerite and chalcopyrite is also important as it can impart galvanic effects to the minerals, affecting flotation.

Currently, studies are done on the use of organic depressants in the depression of millerite. It will be important to study how it would perform on real ore samples as well as understanding the fundamentals of millerite behaviour in more complex systems.

Bibliography

[1] O. Da Silva, “10 Top Nickel Producing Countries | Investing News Network,” 2019. https://investingnews.com/daily/resource-investing/base-metals-investing/nickel-investing/10-top-nickel-producing-countries/ (accessed Oct. 07, 2019).

[2] D. H. Rousell *et al.*, *A Field Guide to the Geology of Sudbury, Ontario*, vol. 6243. 2009.

[3] SPC Metals, “Nickel-Copper-Cobalt-Platinum-Palladium Exploation in the Sudbury Basin,” 2018.

[4] ASM, *ASM specialty handbook: nickel, cobalt, and their alloys*. 2000.

[5] F. K. Crundwell, M. S. Moats, V. Ramachandran, T. G. Robinson, and W. G. Davenport, “Nickel Production, Price, and Extraction Costs,” in *Extractive Metallurgy of Nickel, Cobalt and Platinum Group Metals*, Elsevier, 2011, pp. 21–37.

[6] D. Mondal, G. Villemure, and C. Song, “Synthesis, characterization, and evaluation of unsupported porous NiS submicrometer spheres as a cathode material for lithium batteries,” *J. Appl. Electrochem.*, vol. 44, no. 5, pp. 599–606, 2014, doi: 10.1007/s10800-014-0658-2.

[7] V. Calcutt, “Innovations: Introduction to Copper: Applications,” 2001. https://www.copper.org/publications/newsletters/innovations/2001/08/intro_to_copper.html (accessed Dec. 31, 2020).

[8] U. Shamraiz, A. Hussain, and A. Badshah, “Fabrication and applications of copper sulfide (CuS) nanostructures,” 2016, doi: 10.1016/j.jssc.2016.02.046.

[9] Glencore, “Copper.” https://www.glencore.com/what-we-do/metals-and-minerals/copper (accessed Jun. 23, 2021).

[10] Glencore, “Nickel.” https://www.glencore.ca/en/What-we-do/Metals-and-minerals/Nickel (accessed Oct. 08, 2019).

[11] M. Xu, F. D. Ford, Z. Dai, V. Lawson, C. Mill, and C. Cliff, “PAPER 19 Millerite and Its Impact on Cu / Ni Separation,” *43rd Annu. Meet. Can. Miner. Process.*, no. April, pp. 319–330, 2011.

[12] R. Romero, A. Mazuelos, I. Palencia, and F. Carranza, “Copper recovery from chalcopyrite concentrates by the BRISA process,” doi: 10.1016/S0304-386X(03)00081-1.

[13] W. Holmes and C. N. Operations, “Falconbridge Limited-Strathcona Mill.”

[14] C. Qi *et al.*, “The role of Cu ion activation and surface oxidation for polymorphic pyrrhotite flotation performance in Strathcona Mill,” 2019, doi: 10.1016/j.mineng.2019.01.025.

[15] B. H. L. Andrade, “Potential Use of Oxygen Depleted Air In Nickel Sulphide Flotation,” 2018.

[16] R. R. Moskalyk and A. M. Alfantazi, “Nickel sulphide smelting and electrorefining practice: A review,” *Miner. Process. Extr. Metall. Rev.*, vol. 23, no. 3–4, pp. 141–180, 2002, doi: 10.1080/08827500306893.

[17] G. Kullerud and R. A. Yund, “The Ni-S system and related minerals,” 1962. doi: 10.1093/petrology/3.1.126.

[18] A. E. C. Peres, “The interaction between xanthate and sulphur dioxide in the flotation of nickel-copper sulphide ores,” vol. 1968, 1979, doi: 10.14288/1.0081082.

[19] V. Rajamani and C. T. Prewitt, “The Crystal Structure of Millerite,” *Can. Mineral.*, vol. 12, no. 1, pp. 253–257, 1974.

[20] J. Grice and R. Ferguson, “Crystal structure refinement of millerite (Β-NiS),” *Can. Mineral.*, vol. 12, no. 4, pp. 248–252, 1974, Accessed: Feb. 24, 2020. [Online]. Available: https://pubs.geoscienceworld.org/canmin/article-pdf/12/4/248/4004682/248_12_4_cm.pdf.

[21] H. Sowa, Á. H. Ahsbahs, and Á. W. Schmitz, “X-ray diffraction studies of millerite NiS under non-ambient conditions,” doi: 10.1007/s00269-004-0392-0.

[22] O. Yousfi *et al.*, “Phase transformations in nickel sulphide: Microstructures and mechanisms,” *Acta Mater.*, vol. 58, no. 9, pp. 3367–3380, 2010, doi: 10.1016/j.actamat.2010.02.011.

[23] S. R. Krishnakumar, N. Shanthi, and D. D. Sarma, “Electronic structure of millerite NiS,” *Phys. Rev. B - Condens. Matter Mater. Phys.*, vol. 66, no. 11, pp. 1–6, 2002, doi: 10.1103/PhysRevB.66.115105.

[24] J. Yan, H. Wu, P. li, H. Chen, R. Jiang, and S. (Frank) Liu, “Fe(iii) doped NiS_2 nanosheet: a highly efficient and low-cost hydrogen evolution catalyst,” *J. Mater. Chem. A*, vol. 5, no. 21, pp. 10173–10181, May 2017, doi: 10.1039/C6TA11041J.

[25] W. Mulak, “Kinetics of dissolution of synthetic millerite (β-NiS) in acidic potassium dichromate solutions,” *Hydrometallurgy*, vol. 11, no. 1, pp. 79–89, Aug. 1983, doi: 10.1016/0304-386X(83)90017-8.

[26] G. Pandey, “Synthesis, characterization and optical properties determination of millerite NiS nanorods,” 2012, doi: 10.1016/j.physe.2012.04.015.

[27] C. Clark, “Millerite - Smithsonian Institution.” https://geogallery.si.edu/10002874/millerite (accessed Oct. 09, 2019).

[28] L. K. Smith, G. D. Senior, W. J. Bruckard, and K. J. Davey, “The flotation of millerite - A single mineral study,” *Int. J. Miner. Process.*, vol. 99, no. 1–4, pp. 27–31, May 2011, doi: 10.1016/j.minpro.2011.02.004.

[29] B. Guo, Y. Peng, and R. Espinosa-Gomez, “Cyanide chemistry and its effect on mineral flotation,” *Minerals Engineering*, vol. 66. Elsevier Ltd, pp. 25–32, Nov. 01, 2014, doi: 10.1016/j.mineng.2014.06.010.

[30] G. D. Senior, L. K. Smith, E. Silvester, and W. J. Bruckard, “The flotation of gersdorffite in sulphide nickel systems - A single mineral study,” *Int. J. Miner. Process.*, vol. 93, no. 2, pp. 165–171, Oct. 2009, doi: 10.1016/j.minpro.2009.07.009.

[31] R. S. C. Smart, J. Amarantidis, W. M. Skinner, C. A. Prestidge, L. La Vanier, and S. R. Grano,

Surface Analytical Studies of Oxidation and Collector Adsorption in Sulfide Mineral Flotation, no. May 2014. 2003.

[32] G. P. Power, “The electrochemistry of the nickel sulfides. I. NiS,” 1981. doi: 10.1071/CH9812287.

[33] Y. Peng and S. Zhao, “The effect of surface oxidation of copper sulfide minerals on clay slime coating in flotation,” *Miner. Eng.*, vol. 24, no. 15, pp. 1687–1693, 2011, doi: 10.1016/j.mineng.2011.09.007.

[34] M. Fantauzzi, B. Elsener, D. Atzei, A. Rigoldi, and A. Rossi, “Exploiting XPS for the identification of sulfides and polysulfides †,” 2015, doi: 10.1039/c5ra14915k.

[35] A. M. Helmenstine, “pH Definition and Equation in Chemistry,” 2019. https://www.thoughtco.com/definition-of-ph-in-chemistry-604605 (accessed Jan. 02, 2021).

[36] M. Tayebi-Khorami, E. Manlapig, E. Forbes, M. Edraki, and D. Bradshaw, “Effect of surface oxidation on the flotation response of enargite in a complex ore system,” *Miner. Eng.*, vol. 119, pp. 149–155, Apr. 2018, doi: 10.1016/j.mineng.2018.01.024.

[37] M. C. Fuerstenau and B. J. Sabacky, “On the natural floatability of sulfides,” *Int. J. Miner. Process.*, vol. 8, no. 1, pp. 79–84, 1981, doi: 10.1016/0301-7516(81)90008-9.

[38] Z. Ekmekci and H. Demirel, “Effects of galvanic interaction on collectorless flotation behavior of galena and pyrite,” *Int. J. Miner. Process.*, vol. 52, pp. 31–48, 1997, doi: 10.4028/www.scientific.net/AMR.402.514.

[39] M. Monte, C. R. F. Albuquerque Jr, and A. J. B. Dutra, “Electrochemical Study of the Interaction Galvanic Between Pyrite and Arsenopyrite Through Measurements of Electrode Potentials and Determinations of Contact Angle,” in *ECS Transactions*, Apr. 2006, vol. 2, no. 3, pp. 35–45, doi: 10.1149/1.2195996.

[40] T. V Subrahmanyam and K. S. E. Forssberg, “Mineral solution-interface chemistry in minerals engineering,” *Miner. Eng.*, vol. 6, no. 5, pp. 439–454, 1993, doi: 10.1016/0892-

6875(93)90173-K.

[41] R. C. Hubli, T. K. Mukherjee, S. Venkatachalam, R. G. Bautista, and C. K. Gupta, “Kinetics of millerite dissolution in cupric chloride solutions,” *Hydrometallurgy*, vol. 38, no. 2, pp. 149–159, Jul. 1995, doi: 10.1016/0304-386X(94)00047-7.

[42] J. Liu, Q. Liu, and C. Qi, “Probing the Oxidation of Nickel Sulfide Minerals by the Surface Charge Measurements - Surface Oxidation of Millerite,” 2019.

[43] T. Güler, C. Hicyilmaz, G. Gokagac, and Z. Ekmekci, “Redox Behavior of Chalcopyrite,” *Int. J. Nat. Eng. Sci.*, vol. 3, no. 1, pp. 83–89, 2009.

[44] A. N. Buckley and R. Woods, “An X-Ray photoelectron spectroscopic study of the oxidation of chalcopyrite,” *Aust. J. Chem.*, vol. 37, no. 12, pp. 2403–2413, 1984, doi: 10.1071/CH9842403.

[45] M. Aziz and A. F. Ismail, “X-Ray Photoelectron Spectroscopy (XPS),” in *Membrane Characterization*, 2017.

[46] D. L. Legrand, H. W. Nesbitt, and G. M. Bancroft, “X-ray photoelectron spectroscopic study of a pristine millerite (NiS) surface and the effect of air and water oxidation,” 1998. doi: 10.2138/am-1998-11-1214.

[47] S. Chander, “A brief review of pulp potentials in sulfide flotation,” *Int. J. Miner. Process.*, vol. 72, no. 1–4, pp. 141–150, 2003, doi: 10.1016/S0301-7516(03)00094-2.

[48] X. Cheng and I. Iwasaki, “Pulp Potential and Its Implications to Sulfide Flotation,” *Miner. Process. Extr. Metall. Rev.*, vol. 11, no. 4, pp. 187–210, 1992, doi: 10.1080/08827509208914206.

[49] A. J. Teague, J. S. J. Van Deventer, and C. Swaminathan, “The effect of galvanic interaction on the behaviour of free and refractory gold during froth flotation,” *Int. J. Miner. Process.*, vol. 57, no. 4, pp. 243–263, 1999, doi: 10.1016/S0301-7516(99)00025-3.

[50] Z. Ahmad, “BASIC CONCEPTS IN CORROSION,” in *Principles of Corrosion Engineering and Corrosion Control*, Elsevier, 2006, pp. 9–56.

[51] C. Puente and I. López, “Direct Electrochemical Synthesis of Metal Complexes,” 2018, doi: 10.1016/B978-0-12-811061-4.00003-7.

[52] E. Stamboliadis, “The surface chemistry of the flotation of millerite, pyrrhotite and pentlandite with dialkyl-dithiophosphates,” 1976.

[53] M. Khoshkhoo, M. Dopson, F. Engström, and Å. Sandström, “New insights into the influence of redox potential on chalcopyrite leaching behaviour,” *Miner. Eng.*, vol. 100, pp. 9–16, 2017, doi: 10.1016/j.mineng.2016.10.003.

[54] D. Liu, G. Zhang, J. Liu, G. Pan, Y. Chen, and M. Wang, “Studies on the surface oxidation and its role in the flotation of mixed Cu-Ni sulfide ore,” *Powder Technol.*, vol. 381, pp. 576–584, Mar. 2021, doi: 10.1016/j.powtec.2020.12.038.

[55] M. K. Yelloji Rao, K. A. Natara Jan, and K. A. Natarajan, “Factors Influencing Ball Wear and Flotation With Respect to Ore Grinding,” *Miner. Process. Extr. Metall. Rev.*, vol. 7, no. 4, pp. 137–173, 1991, doi: 10.1080/08827509108952670.

[56] L. Xia, B. Hart, F. Larachi, and O. Gravel, “Galvanic interaction of pyrite with Cu activated sphalerite and its effect on xanthate adsorption,” *Can. J. Chem. Eng.*, vol. 97, no. 10, pp. 2671–2677, Oct. 2019, doi: 10.1002/cjce.23562.

[57] N. N. Elgrishi, K. J. Rountree, B. D. Mccarthy, E. S. Rountree, T. T. Eisenhart, and J. L. Dempsey, “A Practical Beginner’s Guide to Cyclic Voltammetry,” 2017, doi: 10.1021/acs.jchemed.7b00361.

[58] W. Mulak, P. Balaž, and M. Chojnacka, “Chemical and morphological changes of millerite by mechanical activation,” *Int. J. Miner. Process.*, vol. 66, no. 1–4, pp. 233–240, Sep. 2002, doi: 10.1016/S0301-7516(02)00067-4.

[59] J. A. Rumball and G. D. Richmond, “Measurement of oxidation in a base metal flotation circuit by selective leaching with EDTA,” *Int. J. Miner. Process.*, vol. 48, no. 1–2, pp. 1–20, Nov. 1996, doi: 10.1016/s0301-7516(96)00010-5.

[60] P. Clarke, D. Fornasiero, J. Ralston, and R. S. C. Smart, “A study of the removal of

oxidation products from sulfide mineral surfaces," *Miner. Eng.*, vol. 8, no. 11, pp. 1347–1357, 1995, doi: 10.1016/0892-6875(95)00101-U.

[61] H. Gamsjäger, J. Bugajski, R. J. Lemire, and W. Preis, "CHEMICAL THERMODYNAMICS OF NICKEL Tamás GAJDA Deep River ON K0J 1P0 (Canada)," 2005.

[62] Thermo Fisher Scientific, "XPS Interpretation of Carbon." https://xpssimplified.com/elements/carbon.php (accessed Aug. 21, 2020).

[63] D. L. Legrand, G. M. Bancroft, and H. W. Nesbitt, "Surface characterization of pentlandite, (Fe,Ni) 9S8, by X-ray photoelectron spectroscopy," *Int. J. Miner. Process.*, vol. 51, no. 1–4, pp. 217–228, Oct. 1997, doi: 10.1016/S0301-7516(97)00015-X.

[64] G. H. Luttrell and R. H. Yoon, "The collectorless flotation of chalcopyrite ores using sodium sulfide," *Int. J. Miner. Process.*, 1984, doi: 10.1016/0301-7516(84)90048-6.

[65] W. J. Trahar, G. D. Senior, and L. K. Shannon, "Interactions between sulphide minerals - the collectorless flotation of pyrite," *Int. J. Miner. Process.*, vol. 40, no. 3–4, pp. 287–321, 1994, doi: 10.1016/0301-7516(94)90049-3.

[66] Z. Ekmekçi and H. Demirel, "Effects of galvanic interaction on collectorless flotation behaviour of chalcopyrite and pyrite," *Int. J. Miner. Process.*, vol. 52, no. 1, pp. 31–48, 1997, doi: 10.1016/s0301-7516(97)00050-1.

[67] M. J. Nicol, "The electrochemistry of chalcopyrite in alkaline solutions," *Hydrometallurgy*, vol. 187, no. March, pp. 134–140, 2019, doi: 10.1016/j.hydromet.2019.05.016.